Ph.D. DISSERTATION

A STUDY ON WALL-CLUTTER REJECTION TECHNIQUES FOR THROUGH-THE-WALL FMCW RADAR APPLICATIONS

벽투과 FMCW 레이다를 위한 벽클러터 제거 기법에 관한 연구

FEBRUARY 2017

GRADUATE SCHOOL OF ELECTRICAL AND COMPUTER ENGINEERING
SEOUL NATIONAL UNIVERSITY

BYUNGJOON KIM

공학박사 학위논문

A STUDY ON WALL-CLUTTER REJECTION TECHNIQUES FOR THROUGH-THE-WALL FMCW RADAR APPLICATIONS

벽투과 FMCW 레이다를 위한 벽클러터 제거 기법에 관한 연구

2017 년 2 월

서울대학교 대학원

전기 · 정보 공학부

김 병 준

A STUDY ON WALL-CLUTTER REJECTION TECHNIQUES FOR THROUGH-THE-WALL FMCW RADAR APPLICATIONS

지도 교수 남 상 욱

이 논문을 공학박사 학위논문으로 제출함
2017 년 2 월

서울대학교 대학원
전기·정보 공학부
김 병 준

김병준의 공학박사 학위논문을 인준함
2017 년 2 월

위 원 장 서 광 석 (인)

부위원장 남 상 욱 (인)

위 원 정 덕 균 (인)

위 원 김 병 성 (인)

위 원 김 세 윤 (인)

Abstract

This thesis proposes novel wall-clutter rejection techniques and frequency-modulated continuous-wave (FMCW) radar architectures for through-the-wall radar applications. In the through-the-wall radar applications, wall-cutter rejection is very important because the wall-clutter requires high dynamic range of receiver and analog-to-digital converter (ADC). Wideband FMCW radars are good candidates for a high-resolution wall-penetrating detection radar because they can achieve high dynamic range by using a range-gating filter at intermediate frequency or baseband to fully eliminate wall-clutter. However, homodyne FMCW radars require a very high-order high-pass filter (HPF) to fully eliminate wall-clutter when a target is located behind and in close proximity to the wall.

In this thesis, we first investigate a delay-line technique. The inserted delay-line decreases the time-gap between the received signal and the chirp signal. Therefore, the beat-frequencies of the target and wall are shifted to lower frequencies, and the ratio of pass-band to stop-band frequency is increased. As a result, the low-order HPF meets the filter specification. A design methodology and an example for short-range target is provided in this thesis.

And the validity of this technique has been verified with a system simulation.

Even though, the delay-line technique allows the low-order HPF can fully attenuate the wall-clutter, the delay-line in an RF signal path or LO signal path cause several problems: 1) A conventional long delay-line makes considerable signal loss at a high frequency such as X-band or Ka-band; 2) The line-loss also introduces amplitude modulation due to the loss, depending on frequency. Therefore, amplitude modulation increases as radar bandwidth increases, representing a particular problem for high-resolution radar. This amplitude modulation can lead to large side-lobes near a target-beat-frequency; 3) The delay-line requires a large area single-layer substrate or a multi-layer substrate with additional process or expensive process, such as surface acoustic wave (SAW) process to produce a long delay; 4) It is difficult to achieve a controllable delay, from a short delay to a long delay, with a fine time-resolution. It requires abundant delay-lines, control circuits, and loss-compensate circuits, resulting in a bulky system.

Therefore, we propose a novel FMCW radar architecture that employs two phase-locked loops (PLL) and a phase controller. One PLL generates a chirp signal for transmitting (TX chirp) while the other PLL generates a chirp signal for mixing at the mixer (LO

chirp). The PLLs share a reference clock, but the transmitter PLL input path includes a digital phase-controller. When a digital phase control function is activated, the controller advances the reference clock as a half-period by generating one more edge and inversing the following edges. Each reference clock is divided by two and compared to the corresponding PLL's feedback clock. When the phase controller invokes a half-period advance, the transmitter PLL starts tracking. After some cycles, the PLL locks onto the advanced clock, producing a corresponding advanced time in the TX chirp. By repeating this process (advance reference, PLL tracking and PLL locking), it is theoretically possible to produce an infinite time-difference. In practice, due to the finite period of the TX chirp and the LO chirp, the maximum time-difference is limited. This method solves all of the above problems: It does not result in any loss in RF or LO signals, nor produce any amplitude modulation including wideband FMCW radars; does not require greatly increased volume; and permits infinite time-delay with fine time-resolution. This method allows a low-order HPF to highly attenuate wall-clutter and also decouples the relationship between the wall's distance and the HPF's cut-off frequency. The proposed radar was implemented and measured. The wall was located at 1.5 m and the target was located at 3 m at the middle of the room. The measured

results show a second-order HPF attenuates by more than 20 dB for the wall-beat-frequency signal while it does not attenuate the target-beat-frequency signal. The proposed radar is highly appropriate for wall-penetrating detection applications.

Keyword : Frequency-modulated continuous-wave (FMCW) radar, low-order high-pass filter (HPF), phase controller, Two phase-locked loops (PLL), wall-clutter rejection

Student Number : 2009-23088

Table of Contents

Abstract i

Table of Contents v

List of Figures vii

List of Tables xi

Chapter 1. Introduction 1

Chapter 1.1 Radars of the high-resolution wall-penetrating applications 2

Chapter 1.2 Research strategy 5

Chapter 1.3 Dissertation organization 5

Chapter 2. FMCW radar with a delay-line 12

Chapter 2.1 Introduction 13

Chapter 2.2 Design methodology 22

Chapter 2.3 Conclusion 34

Chapter 3. FMCW radar with two PLLs and a digital controller 35

Chapter 3.1 Introduction 37

Chapter 3.2 Design methodology 45

Chapter 3.3 Measurement results 55

Chapter 3.3 Conclusion 60

Chapter 4. Conclusion **61**

Appendix A Wideband DC block design for wideband radar applications **63**

Appendix A.A Introduction 64

Appendix A.B Analysis and design 69

Appendix A.C Implementation and measurements 73

Appendix A.D Conclusion 78

Appendix B FMCW radar components in chap. 3 ..... **79**

Appendix B.A High-pass filter 79

Appendix B.B Chirp source 82

Bibliography **85**

Abstract in Korean **88**

List of Figures

Fig. 1. Wall-penetrating radar 3

Fig. 2. Triangular FMCW radar operation principle..... 5

Fig. 3. Conventional FMCW radar architecture..... 6

Fig. 4. Research strategy 8

Fig. 5. Simulated range profile of a 10 cm thick lossy-dielectric slab in front a 7.62 cm radius cylinder at normal incidence 14

Fig. 6. Wall and target reflection: (a) Dynamic range (20 cm hollow brick) (b) Simulated radar response of a human target at 7 meters behind a 30 cm thick concrete wall..... 15

Fig. 7. The architecture of a wall-penetrating FMCW radar; (a) represents a conventional FMCW radar, (b) represents a FMCW radar with a delay-line 16, 17

Fig. 8. (a) represents mixer-output components with a delay-line (solid line) and without a delay-line (dotted line), and (b) represents a normarlized high-pass filter specification with a delay-line (solid line) and without a delay-line (dotted line) 19

Fig. 9. Ω vs. time-delay graph. Filter order to corresponding

is also plotted. (R_T = 9 m, R_W = 6 m, R_{OC} = 3 m, L_{AW} = 20 dB, L_{AOC} = 30 dB, and C_R = 10,000 GHz/s) 29

Fig. 10. A simulation setup to verify the proposed system (R_T = 9 m, R_W = 6 m, R_{OC} = 3 m, L_{AW} = 20 dB, and L_{AOC} = 30 dB) 31

Fig. 11. Simulation results. Target and wall-clutter with and without filter cases and target and obstacle-clutter with and without filter cases are simulated..... 32

Fig. 12. TX chirp advanced effects. A TX chirp signal (dot-line, black), a LO chirp (solid-line, black), a conventional wall signal (solid-line, blue), and a conventional target signal (solid-line, red), a wall signal with advanced TX chirp (dot-line, blue) and a target signal with advanced TX chirp (dot-line, red)..... 38

Fig. 13. Clocks and PLL response. The reference clock is advanced as half-period when a digital phase control function is activated ("Clock adjusted"). Then, the PLL tracks and locks onto the time-advanced clock. It finally advances the time of the RF signals. In practice, the PLL requires some cycles for locking 40

Fig. 14. A proposed FMCW radar architecture 41

Fig. 15. Fixed radar case. The time-of-flight can be calculated 47

Fig. 16. Non-fixed radar case 49

Fig. 17. HPF design methodology 52

Fig. 18. Measured environment. The wall and the target were middle of the room at 1.5 m and at 3.0 m from radar, respectively. 56

Fig. 19. Measured results. The wall is located at 1.5 m and the target is located at 3 m. Conventional FMCW radar beat-frequency results (black), TX chirp time advanced FMCW radar without HPF beat-frequency results (blue), TX chirp time advanced FMCW radar with HPF beat-frequency results (red) 57

Fig. 20. The proposed DC block. (a) Overall-view, (b) top-view, and bottom-view.....65, 66

Fig. 21. The equivalent circuit of the proposed DC block. .. 67

Fig. 22. The fabricated DC blocks. (a), (c) : 50 and 50 Ω terminated DC block top and bottom view. (b), (d) : 50 and 30 Ω terminated DC block top and bottom view 74

Fig. 23. The simulation and measurement results: 50 and 50 Ω terminated DC block and 50 and 30 Ω terminated DC block 75

Fig. 24. Measurement results. Filter only response (black and red) and filter with mixer response (blue and green) 80

Fig. 25. Phase noise of the PLL. 83

Fig. 26. Output power of the PLL 83

List of Tables

TABLE. I. Design parameters 76

TABLE. II. Comparative summary about the bandwidth, size, impedance transformation, filter type and gap (G_1) of DC blocks 76

Chapter 1

Introduction

Recently, wall-penetrating detection has been an interesting research topic [1]. For through-the-wall high-resolution detection, an ultra-wideband (UWB) short-pulse radar architecture and a wideband frequency-modulated continuous-wave (FMCW) radar architecture can be used. Even though, the UWB short-pulse radar system can be used for high-resolution wall-penetrating detection [2], this architecture must operate at a high peak power or have a high pulse rate frequency in through-wall applications [3]. To achieve high sensitivity and high dynamic range with a low-power operation, a FMCW radar with a range-gating filter can be used to detect targets behind a wall [3], [4].

In chapter 1.1, radars of the high-resolution wall-penetrating applications are described briefly, and the operation principle of the FMCW radar will be discussed in detail. In chapter 1.2, the strategy to overcome the problems. Chapter 1.3 introduces the dissertation organization.

1.1. Radars of the high-resolution wall-penetrating applications

The radar is an abbreviation for radio detection and ranging [5]. Radar systems transmit electromagnetic signals to search for targets. Targets will reflect portions of the incident signals. These reflected signals are received by the radar and processed to extract target information such as range, velocity and angular position.

Historically, radars play an important role in military applications because they can detect long-range targets in poor visibility. As radar design technology and component technologies have been developed in recent years, researchers are attempting to apply radar to a variety of applications such as automotive applications and through-the-wall detection applications as shown in Fig. 1. For through-the-wall high-resolution detection, an UWB short-pulse radar architecture and a wideband FMCW radar architecture can be used. In the both type radars, wall-clutter attenuation is very important because wall-clutter can be much higher than a hidden target signal. The simulated results in the paper [3], 10 cm thick wall-clutter (6.1 m from radar) is approximately 35.8 dB higher than the target signal (9.15 m from

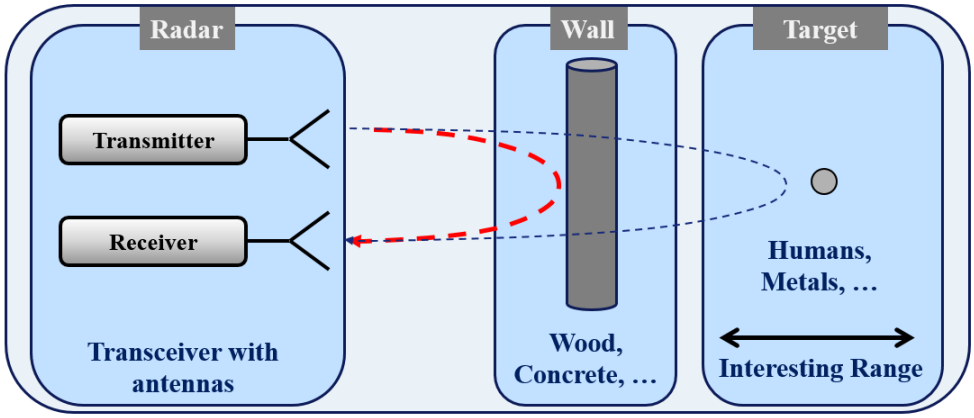

Fig. 1.Wall-penetrating radar.

radar) when using S-band signal. The estimated results in the paper [4], 20 cm thick hollo-bric-wall-clutter is approximately 55 dB higher than the target signal when using L-band signal, while the 30 cm thick concrete-wall-clutter is approximately 70 dB higher than the target signal (7 m).

An UWB short-pulse radar architecture is one of the candidate radar systems for high-resolution wall-penetrating detection [2]. However, this architecture must operate at a high peak power or have a high pulse rate frequency [3] because it uses a short-pulse to achieve high-resolution. Also, it requires a very high-speed ADC (analog-to-digital converter) to receive the short-pulse. To operate the very high-speed ADC, a large power is consumed and it is expensive to implement. To achieve high sensitivity and high dynamic range with a low-power operation, a FMCW radar with a range-gating filter can be used to detect targets behind a wall [3],

[4].

A FMCW radar uses modulated-continuous waveforms such as saw-toothed waveform or triangular waveform. The Fig. 2 shows a triangular waveform FMCW radar operation principle [5]. The radar generates and transmits chirp signals (triangular waveform). As shown in Fig. 2, the generated beat-frequencies, f_B, proportional to the differences between their received signals and their chirp signals. Thus, the beat-frequency is directly proportional to the stationary target range (R). Therefore, the target range can be estimated by measuring the beat-frequency.

$$\Delta t = \frac{2R}{c} \tag{1}$$

$$f_B = \Delta t \cdot C_R = \frac{2R}{c} \cdot C_R \tag{2}$$

where, Δt is the time-of-flight, c is the speed of light, and C_R is the chirp rate.

Short-range clutter has a lower beat-frequency, and long-range clutter has a higher beat-frequency. Therefore, an intermediate frequency (IF) or baseband filter attenuates the clutter. The filter consists of a high-pass filter (HPF) to attenuate

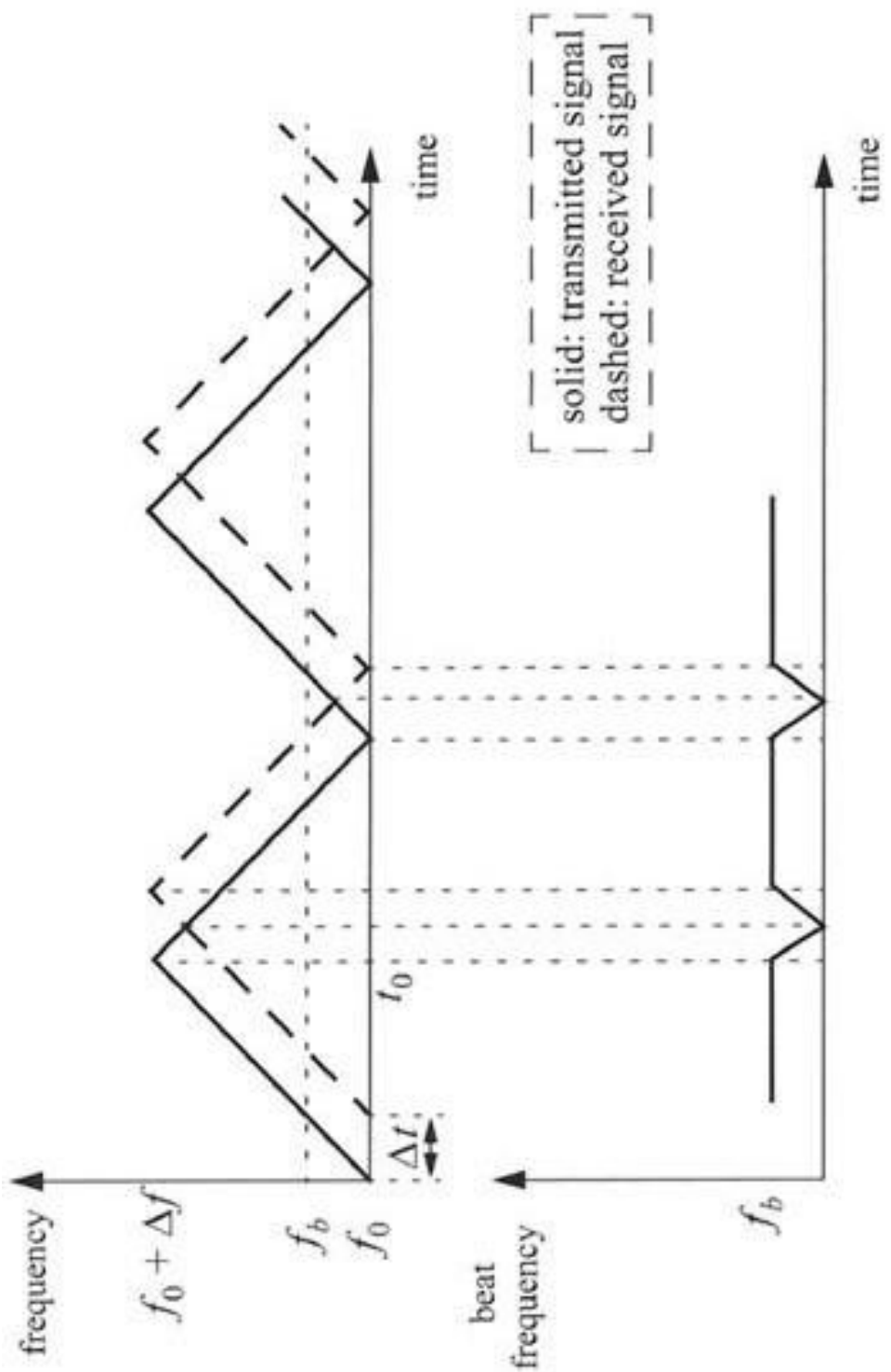

Fig. 2. Triangular FMCW radar operation principle [5].

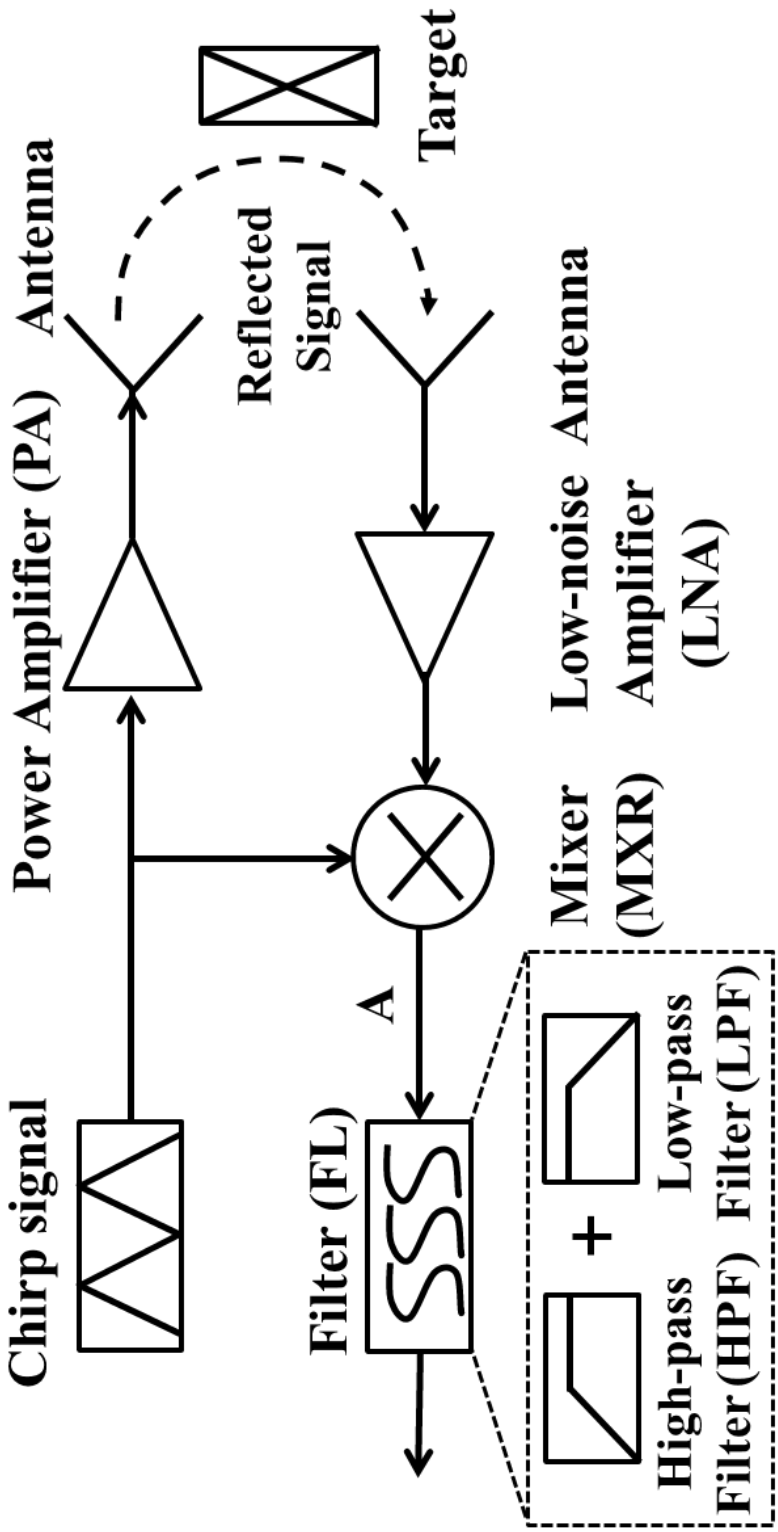

Fig. 3. Conventional FMCW radar architecture [6].

short-range clutter, and a low-pass filter (LPF) to attenuate long-range clutter and high frequency components (HFC) which are generated during the mixing. A conventional FMCW radar architecture is shown in Fig. 3 [6]. However, homodyne FMCW radars require a very high-order high-pass filter (HPF) to fully eliminate wall-clutter when a target is located behind and in close proximity to the wall.

1.2. Research strategy

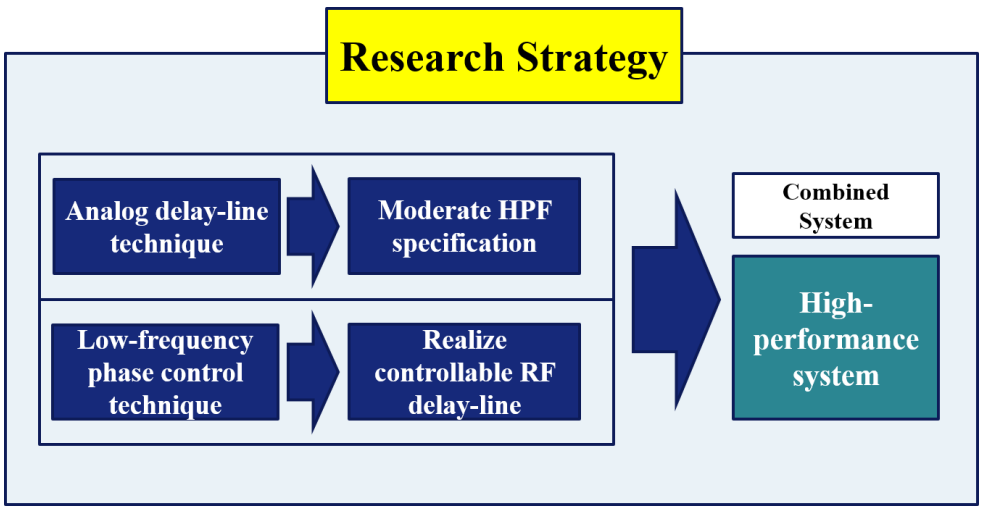

Fig. 4. Research strategy

The research strategy is shown in Fig. 4. To fully eliminate wall-clutter with a low-order HPF, first we investigate a FMCW radar system with an analog delay-line. The delay-line shifts beat-frequencies formed by reflection waves. Therefore, a proper delay moderates HPF specification because the delay increases the ratio of target-beat-frequency to clutter-beat-frequency.

Even though the delay-line in LO path moderates HPF specification, it causes several problems such as loss, distortion, volume and low-reconfigurability. To overcome these problems, we investigate a novel FMCW radar architecture. The proposed radar uses a low-frequency phase control technique to realize artificial controllable delay-line in LO path without true-time delay-lines.

By combining these two techniques, a high-performance low-cost system can be achieved.

1.3. Dissertation organization

In this dissertation, a novel FMCW radar architecture is proposed to attenuate wall-clutter with a low-order HPF. This radar adopts time-difference between transmitter chirp and local-oscillator chirp control concept. To achieve it without true-time delay-lines in radio frequency path, a digitally controllable artificial delay-line concept is developed. To realize an artificial delay-line, a low-frequency phase control technique is used.

In chapter 2, a delay-line effect is investigated in system level to moderate a HPF specification. In this chapter, we assume the delay-line is ideal. Analysis and simulation results show that the effect of the delay-line. The wall-penetrating FMCW radar is considered with and without another short-range clutter.

In chapter 3, a novel FMCW radar system is proposed to realize artificial delay-line. This radar uses two phase-locked-loops (PLL) and a phase controller. By using a PLL's characteristic (Phase-locking) and a low-frequency phase control technique, a digitally controllable artificial delay-line is realized. The measurement results show that the proposed radar can highly attenuate wall-clutter with a low-order HPF.

Chapter 4 describes the conclusion. In this chapter, the effects of the proposed techniques are summarized and the future applications are discussed.

Chapter 2

FMCW radar with a delay-line

In this chapter, we investigate a delay-line effect in a system level. In a wall-penetrating frequency-modulated continuous-wave (FMCW) radar, delay-line adjusts a time-gap between a transmitter chirp (TX chirp) and a local-oscillator chirp (LO chirp). It moderates a high-pass filter (HPF) specification.

FMCW radars are widely used, as they moderate the receiver saturation problem in wall-penetrating applications by attenuating short-range clutter such as wall-clutter. However, conventional FMCW radars require a very high-order HPF to attenuate short-range clutter. A delay-line (DL) is exploited to overcome this problem. Time-delay shifts beat-frequencies formed by reflection waves. This means that a proper time-delay increases the ratio of target-beat-frequency to clutter-beat-frequency. Consequently, low-order HPF fully attenuates short-range clutter. A third-order HPF rejects more than 20 dB and 30 dB for clutter located at 6 m and 3 m, respectively, with a target located at 9 m detection with a 10,000 GHz/s chirp rate and a 28 ns delay-line.

2.1. Introduction

Recently, wall-penetrating imaging has been an interesting research topic [1]. In this applications, wall-clutter reflection is one of important problem because wall-clutter can be much higher than a hidden target signal. The simulated results in the paper [3], 10 cm thick wall-clutter (6.1 m from radar) is approximately 35.8 dB higher than the cylinder metal target signal (9.15 m from radar) when using S-band signal as shown in Fig. 5 The estimated results in the paper [4], 20 cm thick hollo bric-wall-clutter is approximately 55 dB higher than the human target signal when using L-band signal, while the 30 cm thick concrete-wall-clutter is approximately 70 dB higher than the human target signal (7 m) as shown in Fig. 6-(a) and (b).

An ultra-wideband (UWB) short-pulse radar architecture is one of the candidate radar systems for wall-penetrating imaging [2]. However, this architecture must operate at a high peak power or have a high pulse rate frequency in through-wall applications [3]. To achieve high sensitivity and high dynamic range with a low-power operation, a frequency-modulated continuous-wave (FMCW) radar with a range-gating filter as shown in Fig. 7-(a)

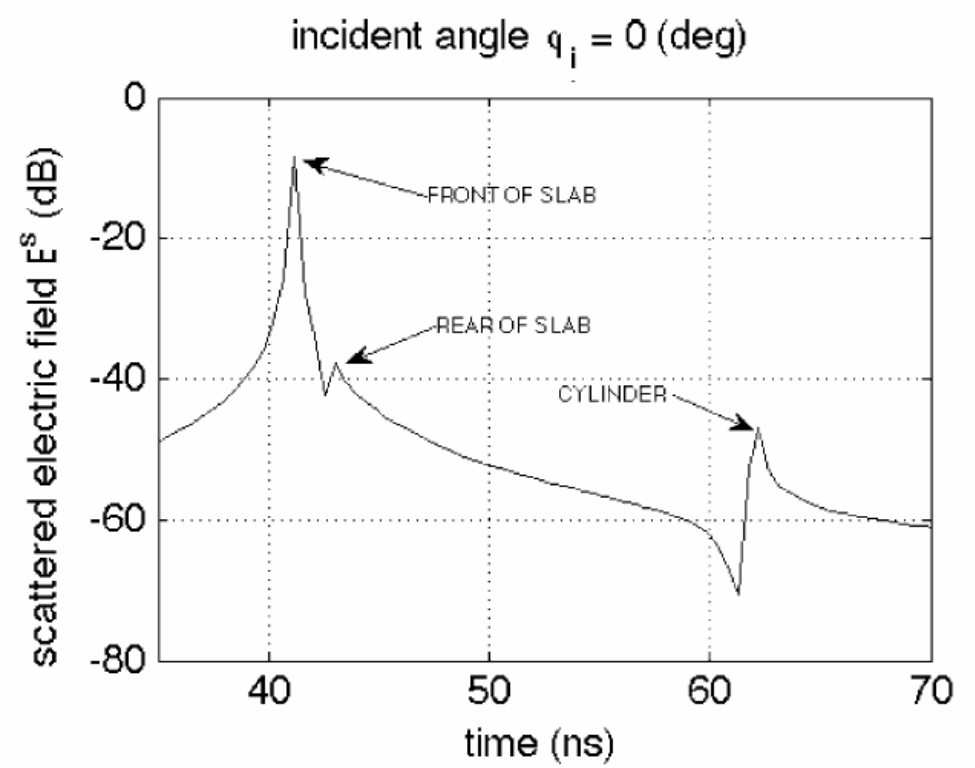

Fig. 5. Simulated range profile of a 10 cm thick lossy-dielectric slab in front a 7.62 cm radius cylinder at normal incidence [3].

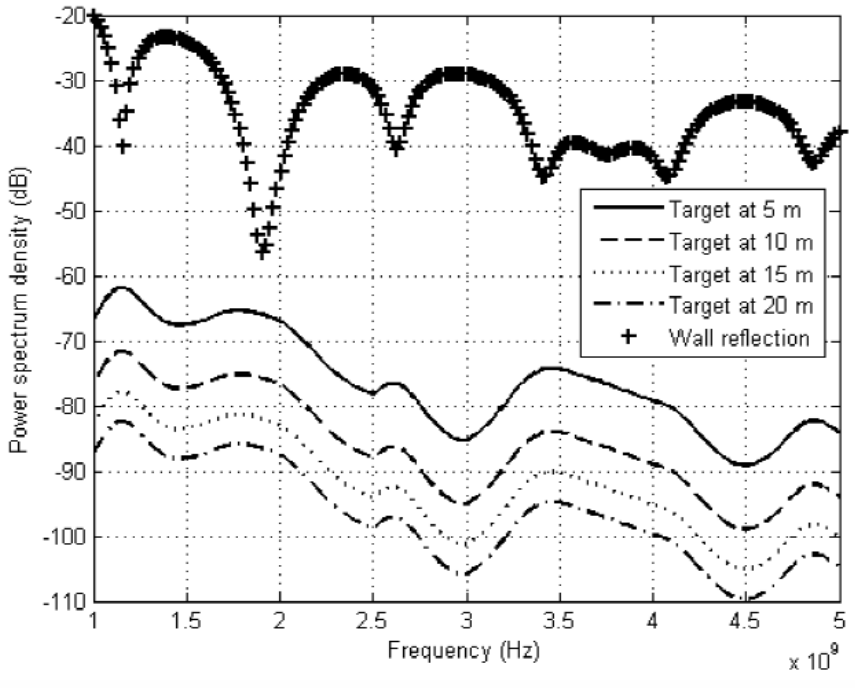

(a)

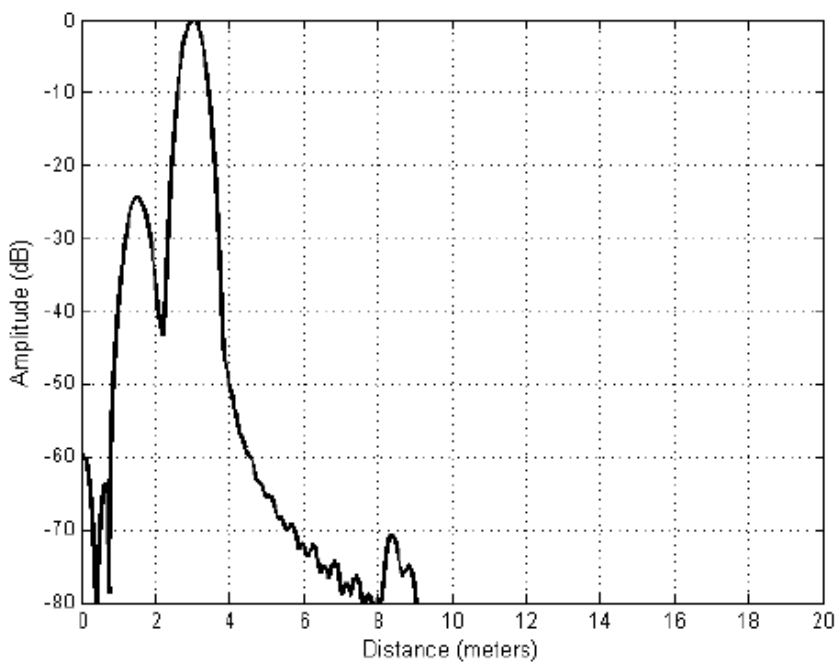

(b)

Fig. 6. Wall and target reflection: (a) Dynamic range (20 cm hollow brick) (b) Simulated radar response of a human target at 7 meters behind a 30 cm thick concrete wall [4].

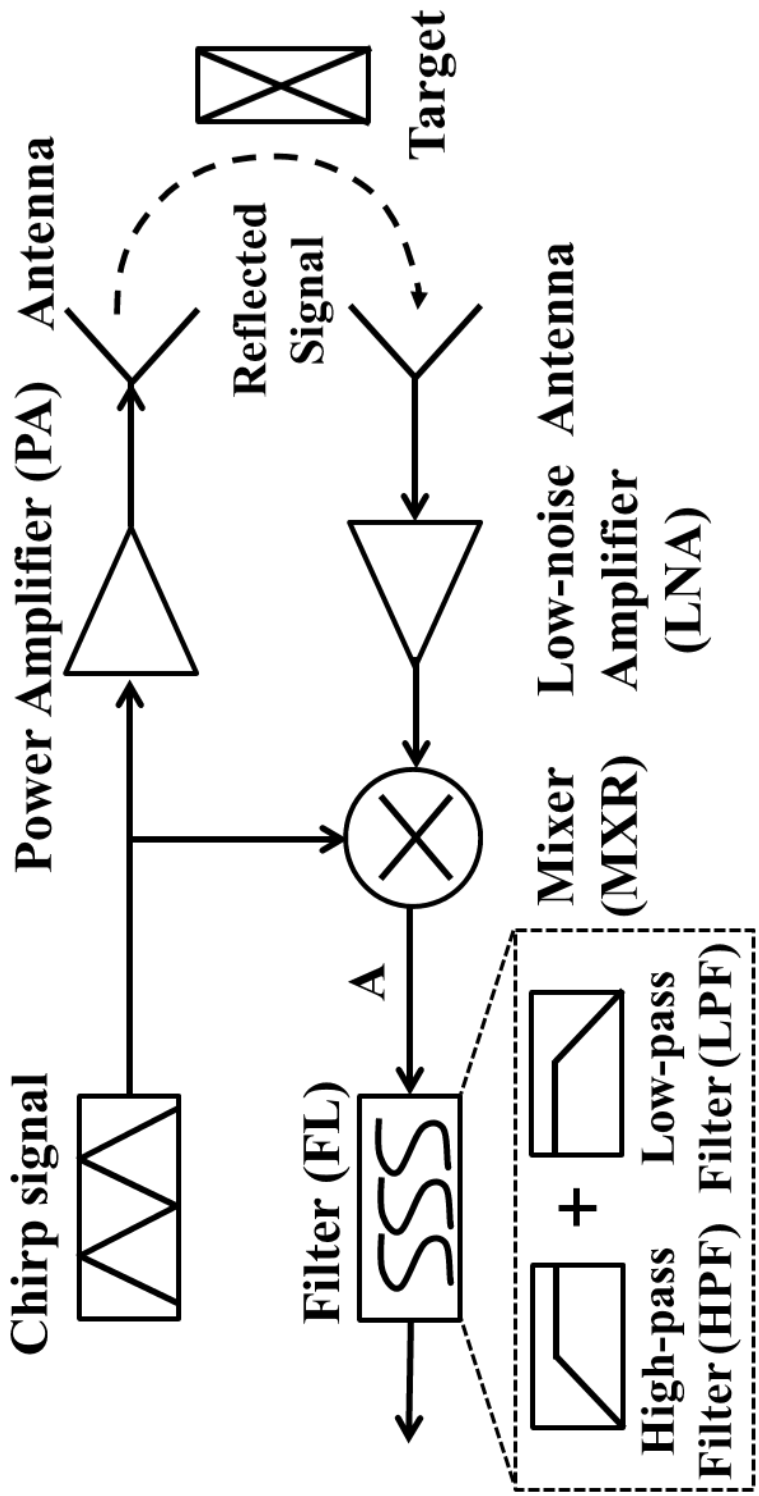
Chirp signal
Power Amplifier (PA)
Antenna
Reflected Signal
Target
Antenna
Low-noise Amplifier (LNA)
Mixer (MXR)
A
Filter (FL)
High-pass Filter (HPF)
+
Low-pass Filter (LPF)

(a)

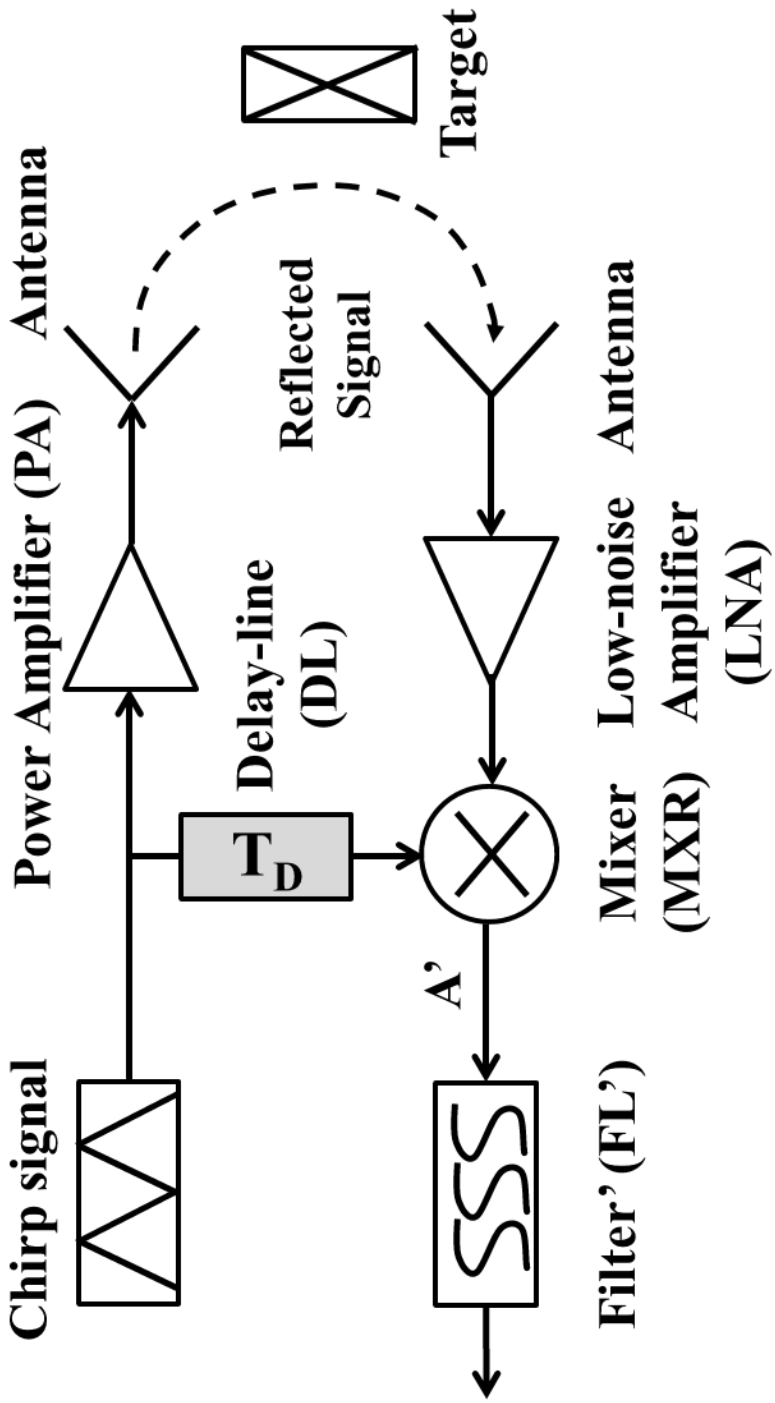

(b)

Fig. 7. The architecture of a wall-penetrating FMCW radar; (a) represents a conventional FMCW radar, (b) represents a FMCW radar with a delay-line [6].

can be used to detect targets behind a wall [3], [4].

FMCW radars generate beat-frequencies proportional to the differences between their received signals and their chirp signals [5]. Thus, the beat-frequency is directly proportional to the stationary target range. Short-range clutter has a lower beat-frequency, and long-range clutter has a higher beat-frequency. Therefore, an intermediate frequency (IF) or baseband filter attenuates the clutter. The filter consists of a high-pass filter (HPF) to attenuate short-range clutter, and a low-pass filter (LPF) to attenuate long-range clutter and high frequency components (HFC) which are generated during the mixing.

However, a very high-order HPF is required to fully attenuate short-range clutter in conventional FMCW radars. To overcome this problem, the present study exploits the delay-line (DL) as shown in Fig. 7-(b).

Delay-lines have already been used in FMCW radars to linearize voltage-controlled oscillator (VCO) [7], identify EM sensor cells [8], and obtain wide-altitude ranges [9]. However, in this thesis, the delay-line is used to attenuate short-range clutter such as wall-clutter with a low-order HPF.

The inserted delay-line decreases the time-gap between the received signal and the chirp signal. Therefore, the beat-

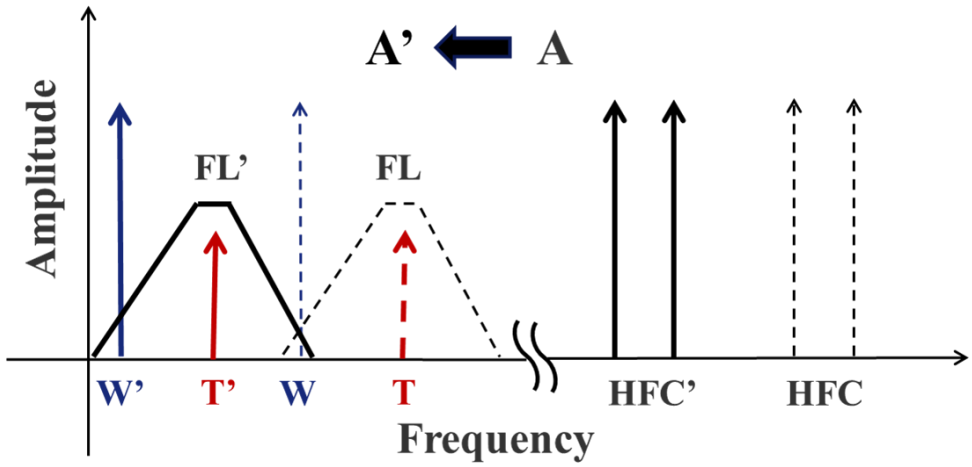

(a)

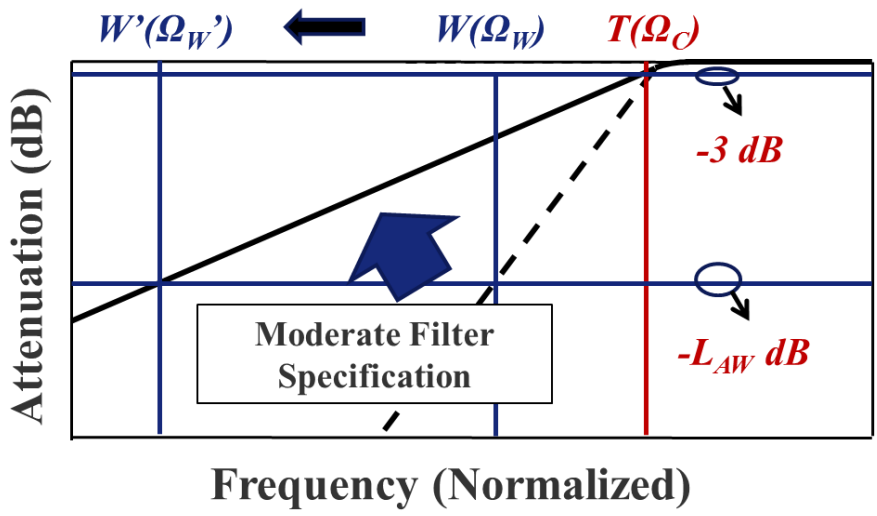

(b)

Fig. 8. (a) represents mixer-output components with a delay-line (solid line) and without a delay-line (dotted line), and (b) represents a normarlized high-pass filter specification with a delay-line (solid line) and without a delay-line (dotted line) [6].

frequencies of the target and wall are shifted to lower frequencies, and the ratio of pass-band to stop-band frequency is increased. As a result, the low-order HPF meets the filter specification, as shown in Fig. 8-(a) and Fig. 8-(b).

In Fig. 8-(a), the dotted line represents the mixer-output components in a conventional FMCW radar, while the solid-line represents the mixer-output components in an FMCW radar with a delay-line. The frequency is shifted constantly by the delay-line so that the wall-beat-frequency, W, changes to W' and the target-beat-frequency, T, changes to T'. As a result, the ratio of target-beat-frequency to wall-beat-frequency increases.

The Fig. 8-(b) shows normalized HPF specifications with a delay-line (solid line) and without a delay-line (dotted line). $T(\Omega_C)$ denotes a normalized filter-cutoff frequency, while $W(\Omega_W)$ and $W'(\Omega_{W'})$ denote a normalized wall frequency without a delay-line and with a delay-line, respectively, and L_{AW} denotes desired attenuation at the wall frequency. As shown in Fig. 5-(b), due to constant frequency shift, the required filter skirt characteristic becomes gradual; this means that a lower order filter can meet the specifications [10].

The following sections explain design methodology, give examples, and present a conclusion. The example is chosen for a

short-range target (a stationary target located at 9 m). It is provided for a public service application in which the radar is installed near the wall and target.

2.2. Design methodology

FMCW radar systems use a beat-frequency to estimate the targets' range [5]. An IF or baseband filter eliminates out-of-range clutter. Therefore, an FMCW radar with an IF filter is highly sensitivity and has a highly dynamic range [3], [4]. Thus, the aforementioned filter is an important component of wall-penetrating FMCW radars.

Such filters consist of LPF and HPF. The LPF attenuates the HFCs generated by the mixer, as well as long-range clutter. The HPF attenuates short-range clutter, such as wall-clutter. In most cases, LPF requirements are low compare with HPF requirements in high-loss wall-penetration applications because the HFCs are far from the target-beat-frequency and long-range clutter is weak due to long-range clutter is attenuated dramatically through air propagation and wall-penetration. For example, when a target is located in the middle of a room with the same Radar Cross Section (RCS) wall at 1 m or at 3 m, the nearby wall-clutter amplitude is roughly larger than 79 dB, based on the assumption of a 30 dB one-way wall-penetration attenuation.

The HPF requirements, conversely, are much more difficult to meet. This is because the nearby wall-clutter and other large

clutter (i.e., high RCS obstacle) located between the radar sensor and the wall can be much stronger than the target signal [4]. Because target is located at the rear of the wall, its amplitude is largely attenuated through wall-penetration, as a result, its amplitude is relatively small compared with such clutter. The radar sensor requires a much higher-order HPF to fully reject this large clutter.

In the following scenario, assume a conventional low-IF FMCW architecture with a target located at R_T, a wall at R_W, and an obstacle at R_{OC}. The IF is f_0, and the chirp rate is C_R. Then, the beat-frequencies are calculated as follows:

$$f_T = f_0 + \frac{2R_T \cdot C_R}{c} \tag{3}$$

$$f_W = f_0 + \frac{2R_W \cdot C_R}{c} \tag{4}$$

$$f_{OC} = f_0 + \frac{2R_{OC} \cdot C_R}{c} \tag{5}$$

where c is the speed of light, f_T is the target's beat-frequency, f_W is the wall's beat-frequency, and f_{OC} is the obstacle's beat-

frequency. Thus, the order of a Butterworth-type HPF can be determined to achieve a desired attenuation [10]:

$$N = \max\{N_W \geq \frac{\log(10^{0.1L_{AW}}-1)}{2log\Omega_W}, N_{OC} \geq \frac{\log(10^{0.1L_{AOC}}-1)}{2log\Omega_{OC}}\} \quad (6)$$

where N is the filter order, N_W and N_{OC} are the filter order needed to achieve the desired attenuation for wall-clutter and obstacle-clutter, respectively, and L_{AW} and L_{AOC} are the minimum attenuations at Ω_W and Ω_{OC}:

$$\Omega_W = \frac{f_0 \cdot \mathrm{c} + 2R_T \cdot C_R}{f_0 \cdot \mathrm{c} + 2R_W \cdot C_R} \quad (7)$$

and

$$\Omega_{OC} = \frac{f_0 \cdot \mathrm{c} + 2R_T \cdot C_R}{f_0 \cdot \mathrm{c} + 2R_{OC} \cdot C_R}. \quad (8)$$

For an example, if an obstacle is 3 m, away, the wall is 6 m away, the target 9 m away, the desirable level attenuation of the wall, L_{AW}, is 20 dB, the desirable level attenuation of the obstacle, L_{AOC}, is 30 dB, the IF, f_0, is 10 MHz, and the chirp rate, C_R, is 800

GHz/s, then $N_W \geq 1{,}441.72$ and $N_{OC} \geq 1{,}082.63$. Consequently, a 1,442th-order Butterworth HPF should be chosen. It is not plausible to implement such a high-order filter, so we must increase both Ω_W and Ω_{OC} so the radar effectively rejects clutter with a low-order filter.

Eq. (7) and Eq. (8) show that high f_0 or low C_R results in low Ω_W and Ω_{OC}, and requires a high-specification HPF. Therefore, a low f_0 or high C_R should be chosen to allow for a low-order HPF. Eq. (7) and Eq. (8) also show that the maximum achievable values are $\Omega_W = R_T/R_W$, and $\Omega_{OC} = R_T/R_{OC}$ when the conditions meet $f_0 \cdot c \ll 2 R_W \cdot C_R$, and $f_0 \cdot c \ll 2 R_{OC} \cdot C_R$.

Unfortunately, the maximum achievable C_R is limited because chirping-control speed is limited by the device and by circuit technology. The C_R is 857 GHz/s in [3] and the C_R is 2000 GHz/s in [4]. In this example, the filter order dropped to 121 when the C_R is 10,000 GHz/s. Even though the filter order dropped to 121, it is still not plausible to implement such a high-order filter. Therefore, it is preferable to set f_0 to zero or to very low; in particular, zero f_0 not only provides the maximum achievable values of Ω_W and Ω_{OC} but also breaks up the relationship between C_R and filter performance. Thus, the best f_0 is zero from an HPF standpoint for suppressing wall-clutter and obstacle-clutter. If f_0 equals zero, Ω_W equals 1.5

and Ω_{OC} equals 3.0 in the above example. Now a 6th-order Butterworth HPF meets the specifications.

However, a 6th-order filter still entails a high implementation cost. To further moderate the filter requirements, a delay-line can be exploited, as shown in Fig. 7-(b). The delay-line decreases the time-gap between a received wave and a chirp signal at mixer and, thus, decreases all beat-frequencies uniformly unless the chirp signal enters the mixer LO-port before the received signal enters to the mixer RF-port. If the arrival time of the two signals is reversed, the larger time-delay increases the beat-frequency because negative beat-frequency folds to become positive. Hence, Eq. (7) and Eq. (8) should be modified to:

$$\Omega_W = \frac{|2R_T - T_D \cdot \mathrm{c}|}{|2R_W - T_D \cdot \mathrm{c}|} \tag{9}$$

and

$$\Omega_{OC} = \frac{|2R_T - T_D \cdot \mathrm{c}|}{|2R_{OC} - T_D \cdot \mathrm{c}|} \tag{10}$$

where T_D is the time-delay at the delay-line. Eq. (9) and Eq. (10) imply that a proper time-delay significantly increases Ω_W and Ω_{OC}.

Therefore, it is possible to implement a radar system that fully attenuates short-range clutter with a low-order HPF.

The delay-line effect is shown in Fig. 8-(a), which depicts how all the beat-frequencies are shifted. In other words, the ratio of the target-beat-frequency to clutter-beat-frequency is increased. As such increased ratio moderates filter specifications, a low-order filter can also meet the attenuation specifications as shown in Fig. 8-(b).

If there is not a large obstacle between the radar and the wall, then the optimum time-delay is equal to $(2R_W)/c$. The Ω_W increases to infinite, and a simple first-order HPF fully rejects wall-clutter. If a large obstacle exists between the radar and the wall, a graphical method can be used to determine the optimum time-delay.

To minimize the filter order, the optimum time-delay makes N_W equal to N_{OC}. Thus, based on Eq. (6), the following is derived:

$$\Omega_{OC} = \Omega_W^A, \tag{11}$$

where $A = \dfrac{\log(10^{0.1L_{AOC}} - 1)}{\log(10^{0.1L_{AW}} - 1)}$.

To find the optimum time-delay for $\Omega_{OC} = \Omega_{WA}$, a graphical

method can be applied directly. The Ω plots versus time-delay, then the $\Omega_{OC} = \Omega_{W^A}$ point is found immediately. The graph in Fig. 9 shows how this works. In the graph, the meeting point between Ω_{OC} (the blue line) and Ω_{W^A} (the red line) represents the optimum time-delay.

In this example, the optimum time-delay is about 28 ns. If we choose a time-delay as 28 ns, the required HPF order is 3. Note that the filter order, N, should be an integer so that the lowest required filter order is 3.

Because the filter order should be an integer, the required filter order remains 3 as long as the time-delay stays within the range of 23 ns to 29 ns. Thus, one is free to choose a time-delay from 23 ns to 29 ns. Notice the required filter order dropped dramatically from 1,442 to 3.

A conventional zero-IF FMCW radar with 10,000 GHz/s chirp rate generates beat-frequencies at 200 kHz, 400 kHz, and 600 kHz from the 3 m obstacle, 6 m wall, and 9 m target, respectively. However, the proposed FMCW radar generates beat-frequencies at 80 kHz, 120 kHz, and 320 kHz due to the 28 ns time-delay shifting all the beat-frequencies. A third-order Butterworth HPF can be designed to attenuate more than 30 dB at 80 kHz, more than 20 dB at 120 kHz, and less than 3.0 dB at 320 kHz.

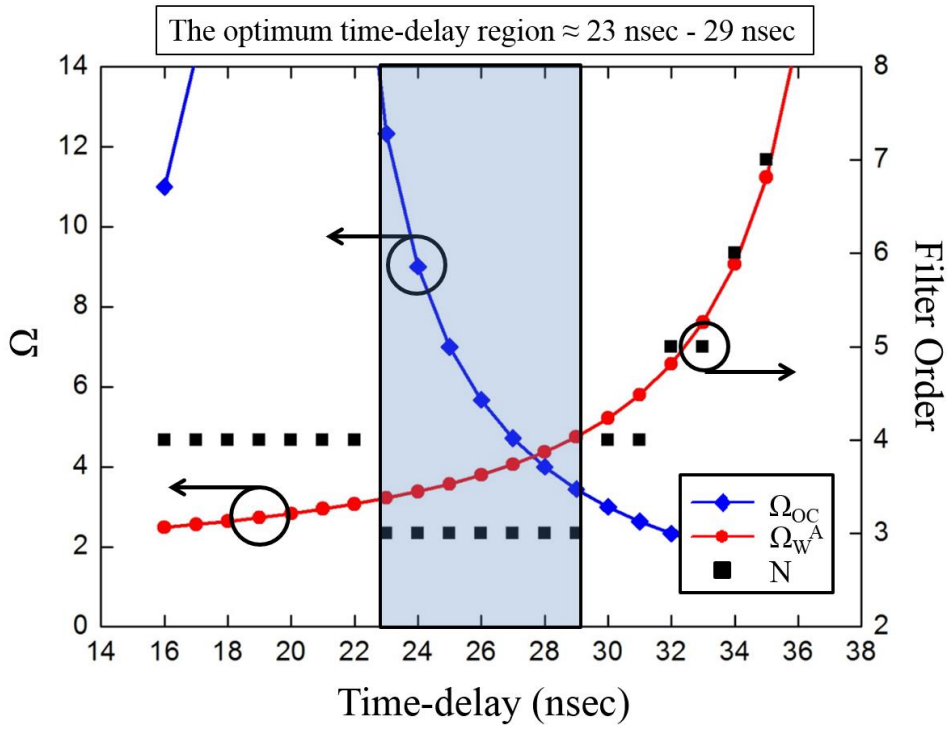

Fig. 9. Ω vs. time−delay graph. Filter order to corresponding is also plotted. (R_T = 9 m, R_W = 6 m, R_{OC} = 3 m, L_{AW} = 20 dB, L_{AOC} = 30 dB, and C_R = 10,000 GHz/s) [6].

This has been verified via a system simulation using the Advanced Design System (ADS) [11]. A simulation setup is shown in Fig. 10. An ideal voltage source generates an ideal triangular voltage (0−1 V with 400 μs up/down speed, at node A). Thus, the ideal VCO generates a chirp signal (100 MHz–4100 MHz, at node B). A splitter (SPL1) splits the signal two ways, sending one signal into the LO−port of the mixer (MXR) and the other into another splitter (SPL2). The SPL2 again splits the signal in two, one signal representing clutter, and the other representing a target. These signal delays corresponding to range. Time−delay components (TD−2, TD−3) are used to represent a target and a wall or an obstacle. TD−3 is set to 60 ns to represent a 9 m target, and TD−2 is set to 40 ns to represent a 6 m wall or is set to 20 ns to represent a 3 m obstacle. The time−delay component (TD−1) represents a delay−line used to moderate filter specifications. It is set to 28 ns, which is the optimum delay for minimizing HPF order. The optimum delay is obtained by using the provided design methodology. The simulation results are shown in Fig. 11. When the same power signals (target and clutter) are injected, the target signal is decreased by 2.8 dB, the wall signal is decreased by 24.0 dB, and the obstacle signal is decreased by 36.4 dB. These results show sound agreement with the theory.

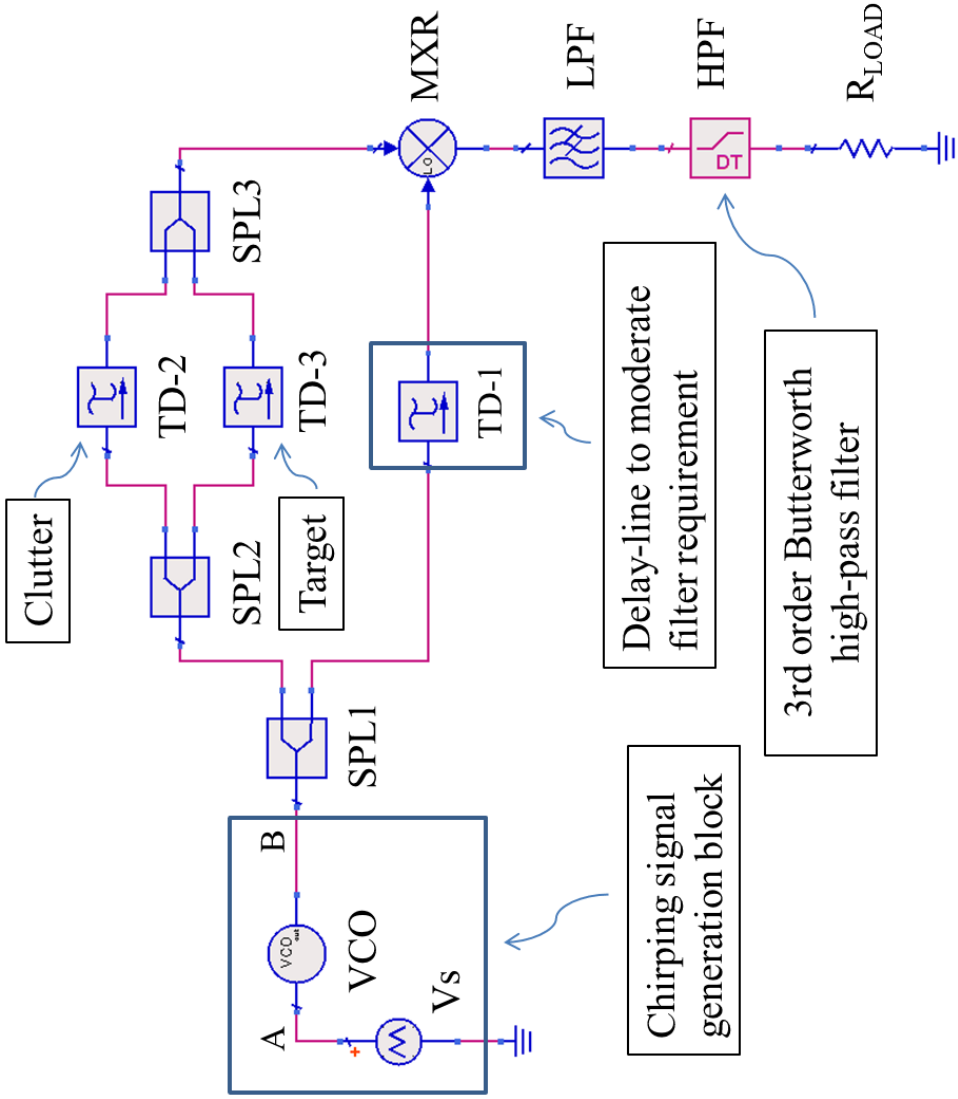

Fig. 10. A simulation setup to verify the proposed system.
(R_T = 9 m, R_W = 6 m, R_{OC} = 3 m, L_{AW} = 20 dB, and L_{AOC} = 30 dB) [6].

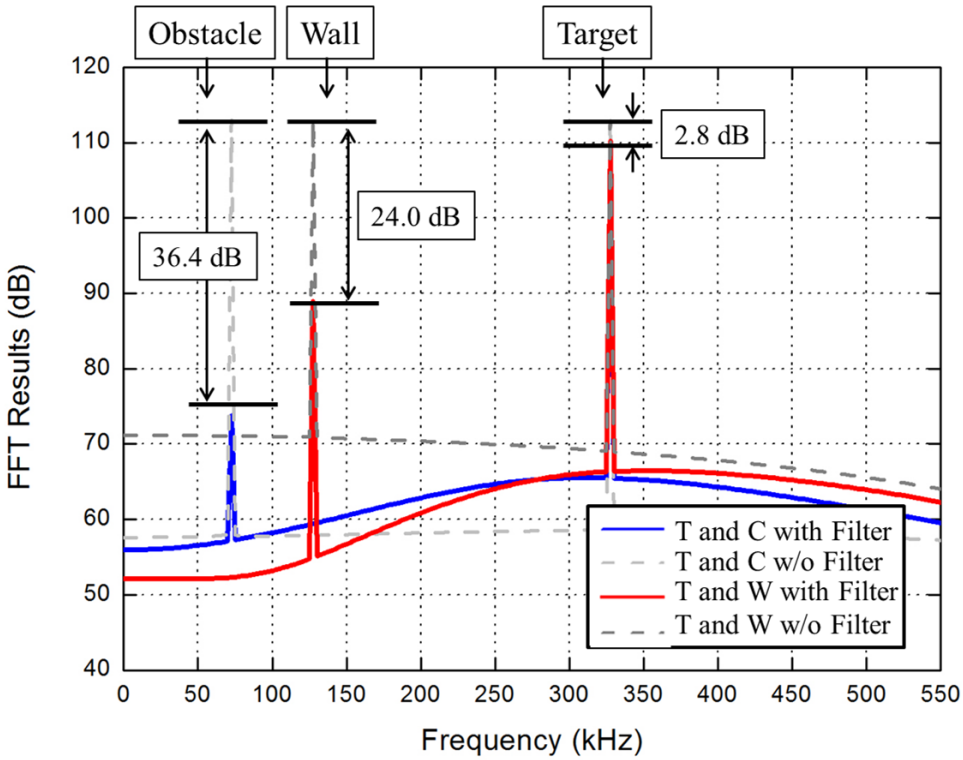

Fig. 11. Simulation results. Target and wall−clutter with and without filter cases and target and obstacle−clutter with and without filter cases are simulated [6].

Note that this is assuming the wall and the short-range obstacle locations are already known or have been measured using radar. Also, the technique discussed assumes the target is stationary. Yet, the technique can be applied to a variety of scenarios including moving target scenarios. In fact, as this technique constantly shifts the beat-frequencies, the filtered-out signals are only frequency shifted compare with the conventional FMCW radars. Existing processing and algorithms for the conventional FMCW radars (e.g., Doppler processing or Imaging algorithms) can be applied to an FMCW radar with a delay-line simply by compensating for frequency shifting.

Note that some FMCW radar has a finite antenna isolation with a certain time-delay. In this case, a finite antenna isolation can be understood as an obstacle (short-range clutter) in the given example. Therefore, a high isolation between a transmit antenna and a receiver antenna is desirable.

2.3. Conclusion

In this chapter, a short-range clutter rejection technique is proposed for wall-penetrating FMCW radar. This method requires only the addition of a simple delay-line at the receiver LO-port to control the time difference between chirp and received signals at the mixer. It allows a low-order HPF to fully attenuate short-range clutter. The validity of this has been verified with a system simulation. This study will help further the implementation of the FMCW radar in wall-penetrating applications.

Chapter 3.

FMCW radar with two PLLs and a digital controller

In this chapter, we proposes a novel frequency-modulated continuous-wave (FMCW) radar to achieve high wall-clutter rejection with a low-order high-pass filter (HPF). The proposed radar has two phase-locked loops (PLL) and a phase controller. One transmitter PLL generates a chirp signal for transmitting (TX chirp) signal, the other a local-oscillator PLL generates a chirp signal for mixing (LO chirp), and the phase controller control a phase of a reference clock entering the transmitter PLL. When the phase controller advances by a half-period of the reference clock, the PLL tracks and locks onto the advanced reference clock, and the TX chirp signal is advanced by a half-period of the reference clock. If longer advanced time is needed, the above process (advance, track, and lock) is repeated after PLL locking. In this manner, long advanced time can be achieved with a fine time-resolution. The use of appropriate advanced time decreases the time-gap between a wall-reflection signal and the LO chirp signal, and increases the ratio of target-beat-frequency to wall-beat-

frequency. This enables a low-order HPF to fully attenuate wall-clutter. Moreover, this technique decouples the relationship between the wall's distance and the HPF's cut-off frequency. The radar was implemented and measured. The wall was located at 1.5 m and the target was located at 3 m. The measured results show a second-order HPF attenuates by more than 20 dB for the wall-beat-frequency signal while it does not attenuate the target-beat-frequency signal.

3.1. Introduction

Within the recent years, wall-penetrating radar has gained attention from researchers [1-3], [12]. Wideband frequency-modulated continuous-wave (FMCW) radars are good candidates for a high-resolution wall-penetrating detection radar [3], [12]. FMCW radar achieves high dynamic range by using a range-gating filter at intermediate frequency or baseband to fully eliminate wall-clutter. However, homodyne FMCW radars require a very high-order high-pass filter (HPF) to fully eliminate wall-clutter when a target is located behind and in close proximity to the wall [6]. To overcome this problem, a delay-line is exploited in [6]; this delays a chirp signal, which enters a mixer local-oscillator (LO) port (LO chirp), and reduces the time-gap between a received signal and the chirp signal. Consequently, the ratio of target-beat-frequency to wall-beat-frequency increases and a low-order HPF fully eliminates wall-clutter. It is equivalent to the transmitter chirp (TX chirp) being time-advanced, as shown in Fig. 12 (where f_T and f_T' are target-beat-frequency, and f_W and f_W' are wall-beat-frequency). Note that if the time-gap is zero, then the wall-beat-frequency is zero.

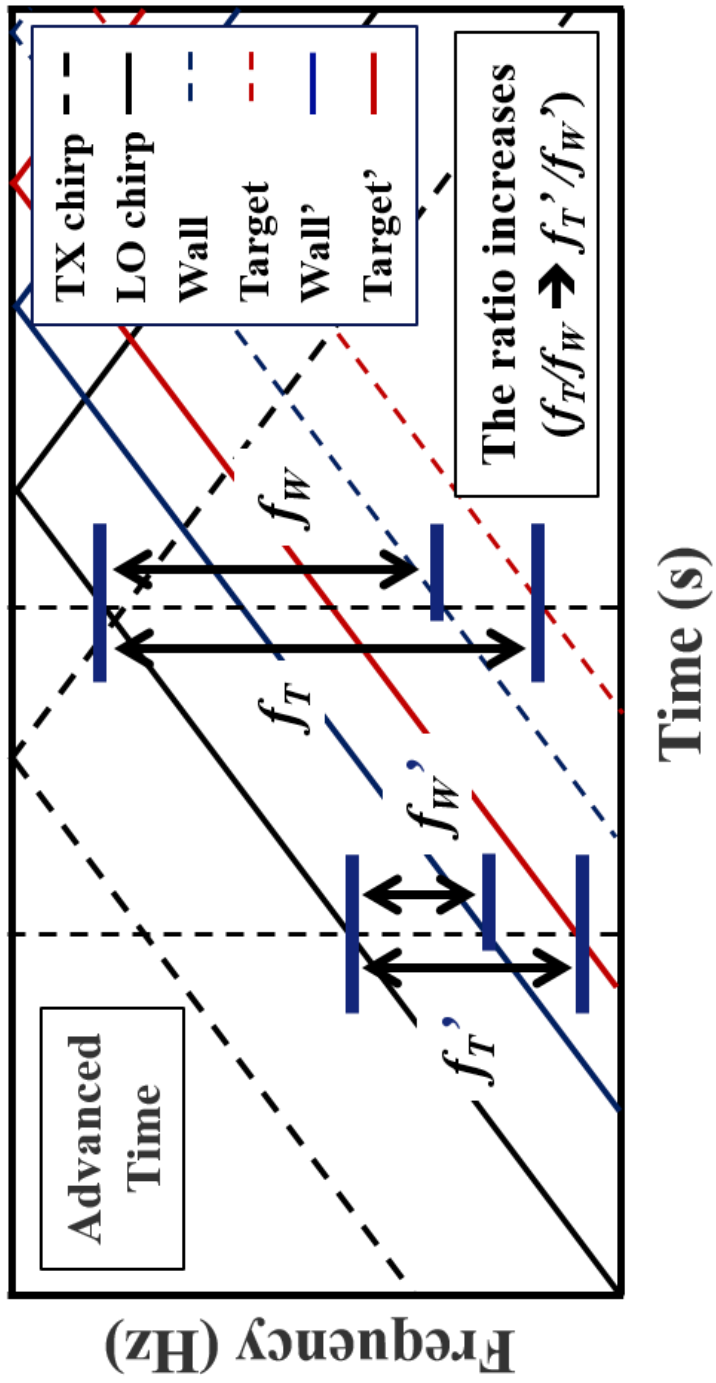

Fig. 12. TX chirp advanced effects. A TX chirp signal (dot-line, black), a LO chirp (solid-line, black), a conventional wall signal (solid-line, blue), and a conventional target signal (solid-line, red), a wall signal with advanced TX chirp (dot-line, blue) and a target signal with advanced TX chirp (dot-line, red) [15].

Delay-lines have been exploited in FMCW radars, to delay a radio-frequency (RF) signal or LO signal [6-9]. However, delay-lines in an RF signal path or LO signal path invoke several problems: 1) A conventional long delay-line makes considerable signal loss at a high frequency such as X-band or Ka-band [13]. It additionally requires high-frequency amplifiers; 2) The line-loss also introduces amplitude modulation due to the loss, depending on frequency. Therefore, amplitude modulation increases as radar bandwidth increases, representing a particular problem for high-resolution radar. This amplitude modulation can lead to large side-lobes near a target-beat-frequency [14]; 3) The delay-line requires a large volume to produce a long delay. For example, to achieve a delay of several hundred nanoseconds, a micro-strip line of several meters long is required on a conventional substrate [13]; alternatively, a multi-layer substrate with additional process or expensive process, such as surface acoustic wave (SAW) process, is required [7]; 4) It is difficult to achieve a controllable delay, from a short delay to a long delay, with a fine time-resolution. It requires abundant delay-lines, control circuits, and loss-compensate circuits, resulting in a bulky system.

In order to remove true-time delay-lines in RF or LO path, digital techniques can be used. These techniques create the original

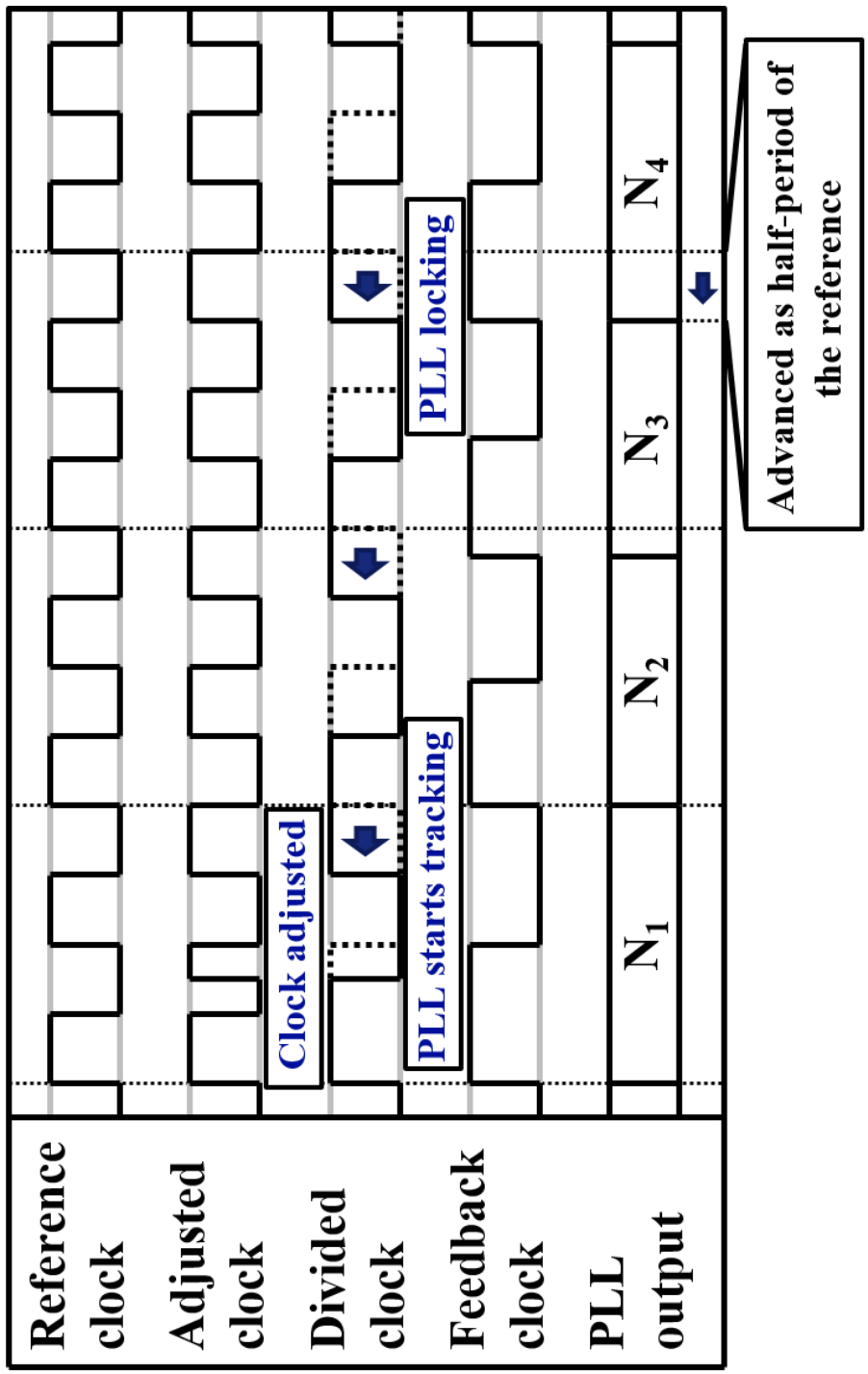

Fig. 13. Clocks and PLL response. The reference clock is advanced as half-period when a digital phase control function is activated ("Clock adjusted"). Then, the PLL tracks and locks onto the time-advanced clock. It finally advances the time of the RF signals. In practice, the PLL requires some cycles for locking [15].

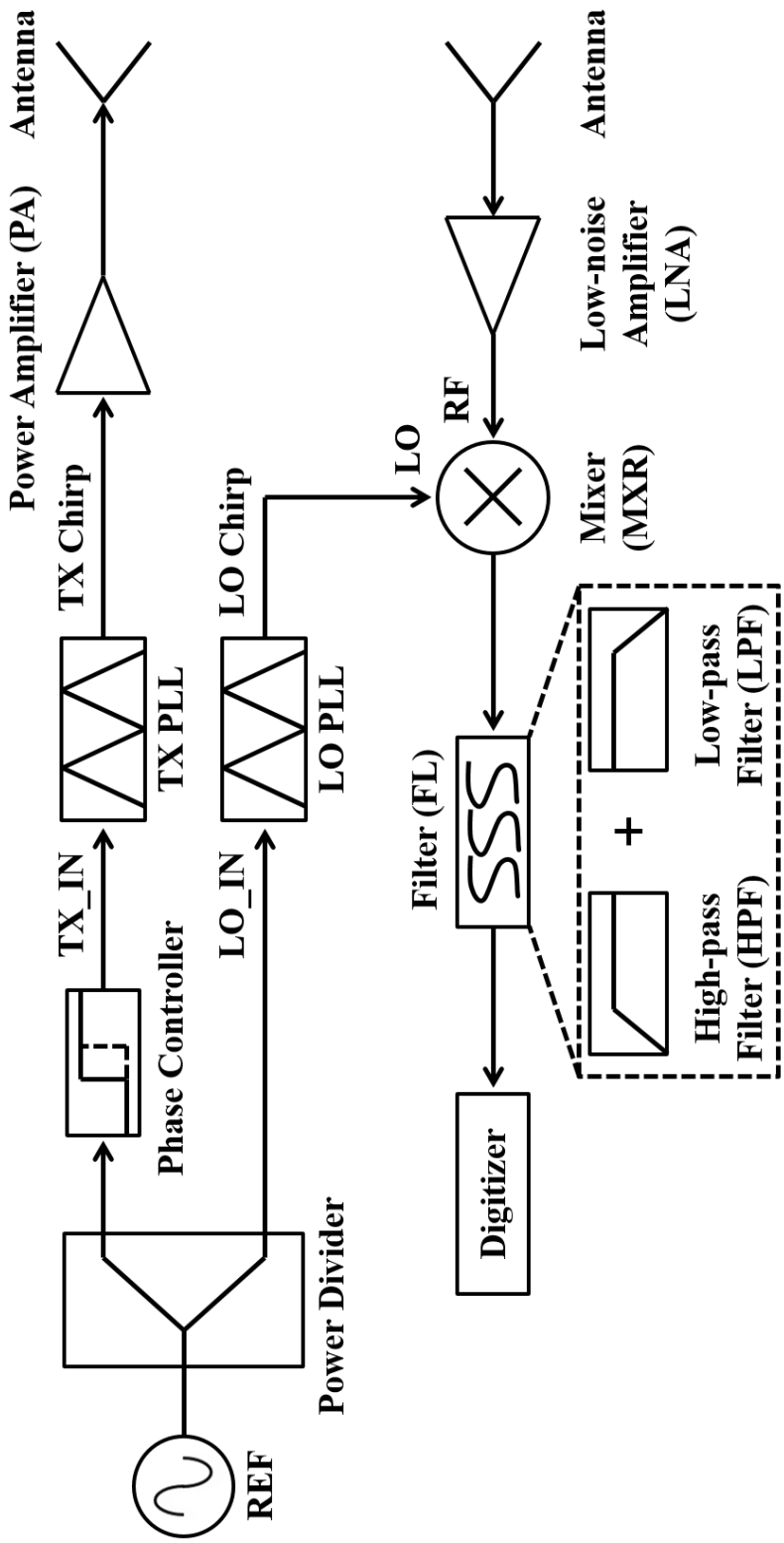

Fig. 14. A proposed FMCW radar architecture [15].

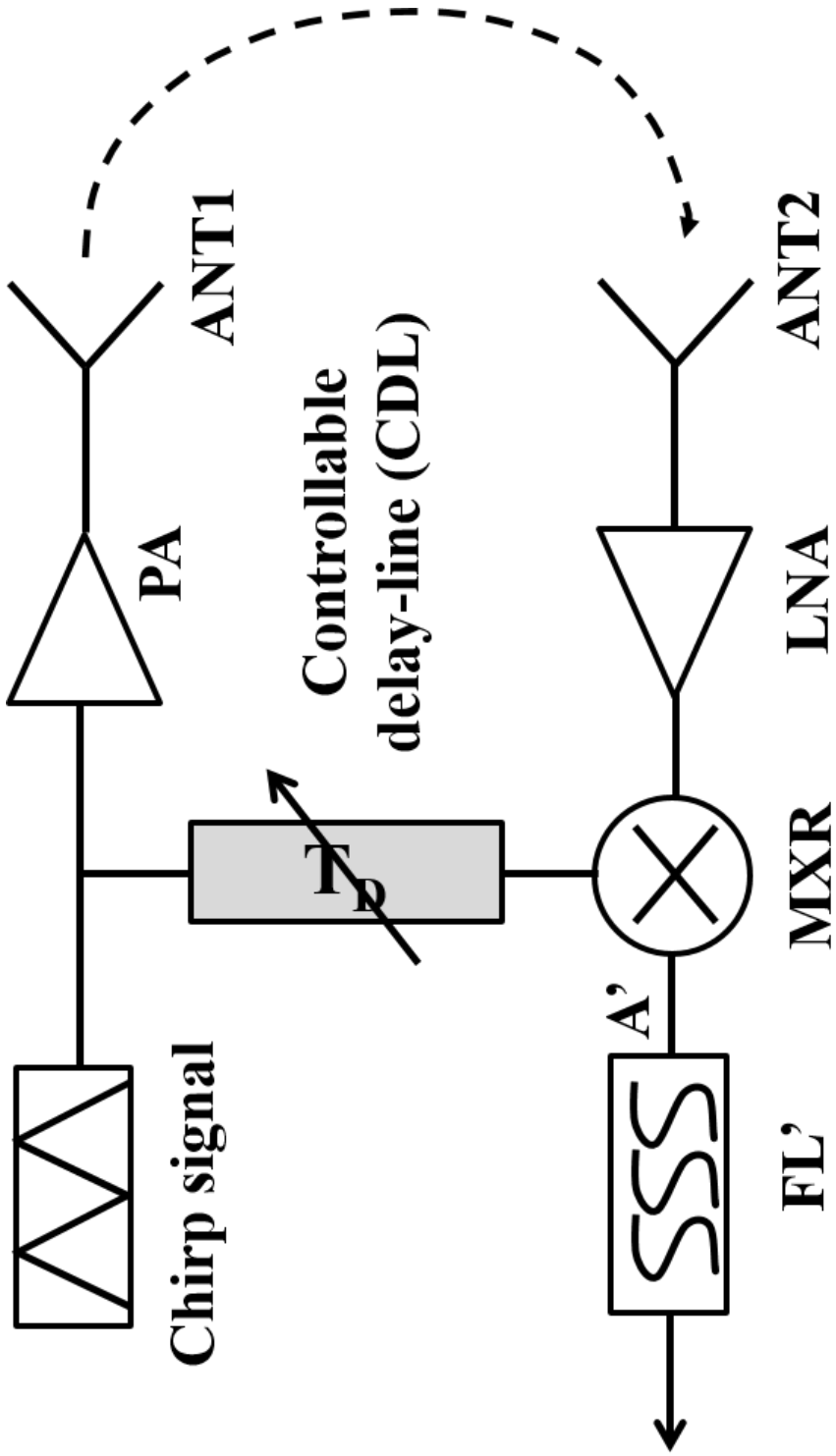

Fig. 15. The equivalent system [15].

chirp and its replica entirely digitally. These radars have several advantages. The amplitude and the phase distortions occurring during the mixing process can be compensated by pre-distortion. And it can be easily controlled. However, to generate high frequency wideband chirp signals, it requires large power or additional blocks such as multipliers. It increases costs and complexity. Therefore, we propose a novel FMCW radar architecture that employs two phase-locked loops (PLL) and a phase controller, as shown in Fig. 13 and 14. One PLL generates a chirp signal for transmitting (TX chirp) while the other PLL generates a chirp signal for mixing at the mixer (LO chirp). The PLLs share a reference clock, but the transmitter PLL input path includes a digital phase-controller. When a digital phase control function is activated, the controller advances the reference clock as a half-period by generating one more edge and inversing the following edges, as shown in Fig. 13. Each reference clock is divided by two and compared to the corresponding PLL's feedback clock. When the phase controller invokes a half-period advance, the transmitter PLL starts tracking. After some cycles, the PLL locks onto the advanced clock, producing a corresponding advanced time in the TX chirp. By repeating this process (advance reference, PLL tracking and PLL locking), it is theoretically possible to produce an

infinite time-difference. In practice, due to the finite period of the TX chirp and the LO chirp, the maximum time-difference is limited. This method solves all of the above problems: It does not result in any loss in RF or LO signals, nor produce any amplitude modulation including wideband FMCW radars; does not require greatly increased volume; and permits infinite time-delay with fine time-resolution. The equivalent system is shown in Fig. 15.

This method allows a low-order HPF to highly attenuate wall-clutter and also decouples the relationship between the wall's distance and the HPF's cut-off frequency. The following sections provide a more detailed description and measurement results. Section 3.2 provides the design methodology, Section 3.3 provides measurement results, and Section 3.4 presents the conclusions.

3.2. Design methodology

In conventional homodyne FMCW radars that detect a target behind a wall, a very high-order HPF should be imposed to fully eliminate wall-clutter [6].

To moderates the HPF specification, a novel FMCW radar architecture is proposed, as shown in Fig. 14. One PLL (TX PLL) produces a chirp signal for transmitting (TX chirp) and a second PLL (LO PLL) produces a chirp signal for mixing (LO chirp). If there is a proper constant time-advance of the TX chirp compared to the LO chirp, then the time-gap between the received signal and the LO chirp decreases. Consequently, the beat-frequencies of the wall and of the target decrease, which are calculated as follows:

$$f_T' = (\frac{2R_T}{c} - \tau)C_R \tag{12}$$

and

$$f_W' = (\frac{2R_W}{c} - \tau)C_R \tag{13}$$

where f_T' is the target's beat-frequency, f_W' is the wall's beat-frequency, R_T is the target's distance, R_W is the wall's distance, c is the speed of light, τ is the time-advance, and C_R is the chirp rate. Note that when the time-advance equals the time-of-flight of the wall, $2R_W/c$, then the wall-beat-frequency goes to zero and a simple first-order HPF or a DC block capacitor fully rejects the wall-clutter.

As explained above, the two PLLs and the phase controller allow for a specific time-shift. Note that time-shifting is quantized with a specific time-resolution. A higher reference frequency provides a higher time-resolution.

From the HPF standpoint, a high frequency is preferred to achieve a very fine time-resolution, in order to reduce the wall-beat-frequency to zero or a very low frequency. For example, radar with a 25,000 GHz/s chirp rate detects a target located at 3 m, and a wall located at 1.5 m. If the reference frequency is 10 GHz, then the half-period is 50 ps. By repeating the half-period time-advance function, the TX chirp has a 10 ns time-advance. Then, the beat-frequency of the wall decreases to zero, and that of the target decreases to 250 kHz. Then, a first-order HPF fully attenuates the wall-clutter whereas it attenuates the target by less than 3 dB [10]. However, it is important to select an appropriate input reference

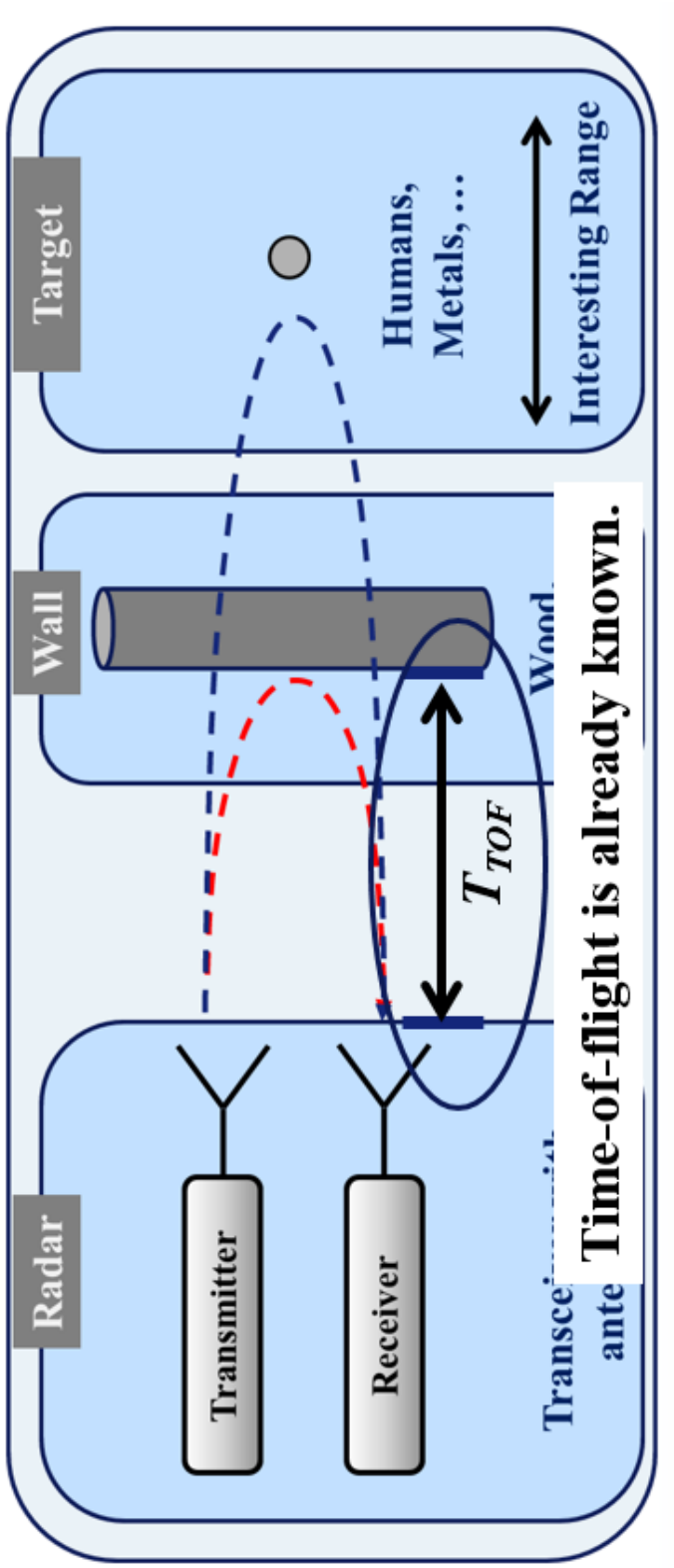

Fig. 15. Fixed radar – The time−of−flight can be calculated.

frequency. Such a high frequency (10 GHz) increases the complexity of the design and implementation of components for phase-shifting, increases the costs and power requirement of components, and makes it difficult to achieve a stable, high-quality, low-cost reference source.

If the proposed technique is applied to a radar system positioned at a specific location and with a fixed radar-wall distance, the reference clock frequency is easily determined. Because the distance is fixed, the time-of-flight of the wall and the required time-advance can be precisely calculated as shown in Fig. 15. The time-resolution is chosen either by the equivalent of the calculated wall time-of-flight or the calculated value divided by an integer. The period of the reference clock is set to double the time-resolution. For example, if the radar-wall distance is 4.5 m, then the time-of-flight is 30 ns. The time-resolution can be selected as 30 ns, 15 ns, 7.5 ns, etc. For time-resolution of 15 ns, the period of the reference clock is 30 ns and the corresponding frequency is 33.333 MHz.

If the technique is applied to non-fixed radars as shown in Fig. 16, the reference clock frequency should be determined more carefully because the radar-wall distance is not fixed. For example, radar that uses a 50 MHz reference frequency can dramatically

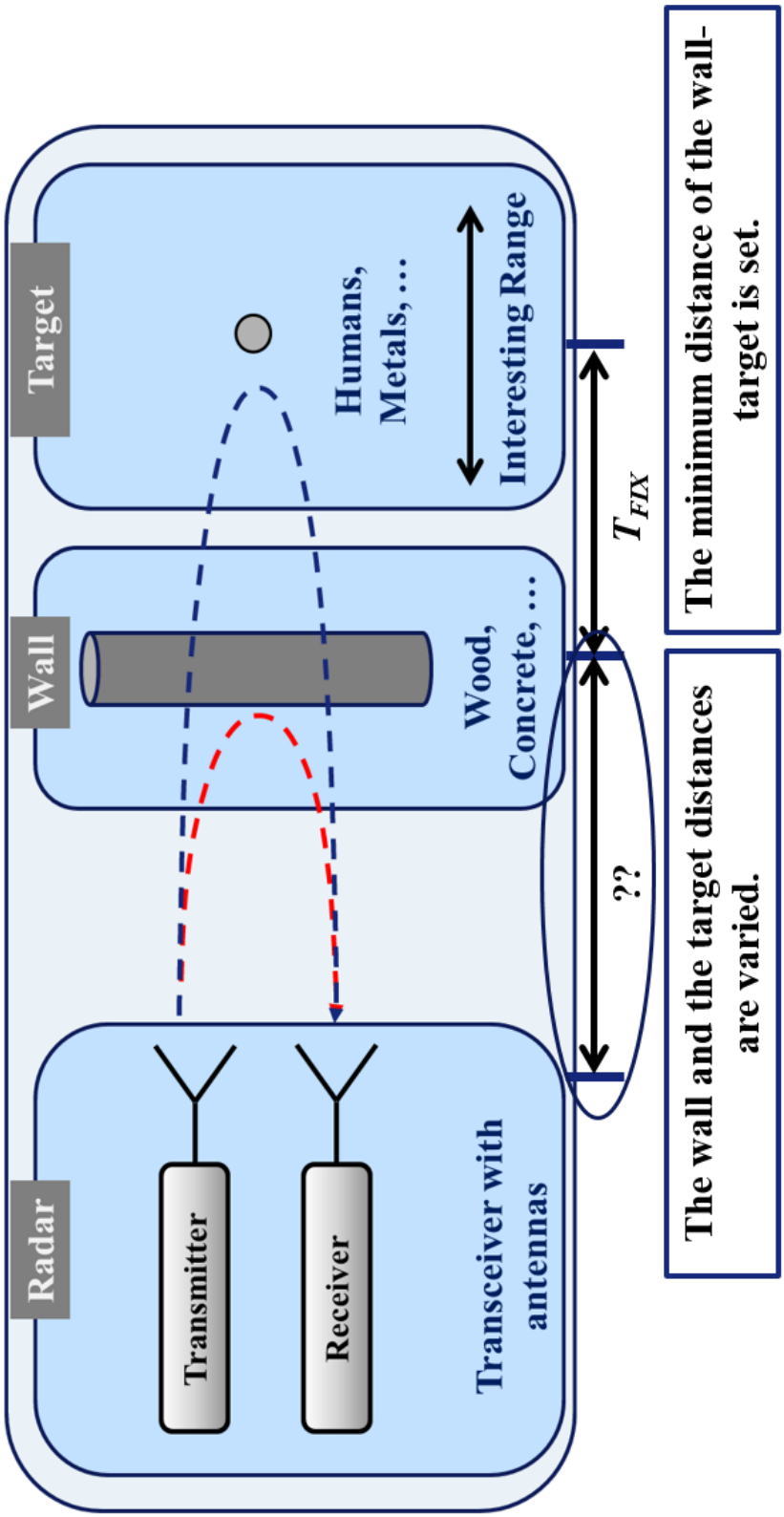

Fig. 16. Non-fixed radar.

reduce the beat-frequency of a wall at 1.5 m but not at 1.0 m.

In order to achieve the lowest HPF order, we must maximize the ratio of target-beat-frequency to wall-beat-frequency, r, as calculated below:

$$r = \frac{f_T'}{f_W'} = \frac{2R_T - \tau c}{2R_W - \tau c} \quad \text{for} \quad 0 \le \tau \le \frac{2R_W}{c}, \tag{14}$$

$$r = \frac{f_T'}{f_W'} = \frac{2R_T - \tau c}{\tau c - 2R_W} \quad \text{for} \quad \frac{2R_W}{c} < \tau, \tag{15}$$

$$\text{where } \tau = T_{RES}N, \tag{16}$$

T_{RES} is the time-resolution and N is an integer. The time-advance is quantized because N is an integer.

Because Eq. (14) is a monotonically increasing function, the ratio increases as the time-advance increases unless the time-advance does not exceed the time-of-flight of the wall. Otherwise, the ratio decreases as the time-advance increases when the time-advance exceeds the time-of-flight of the wall. Therefore, N_O or $N_O + 1$ is the optimum value and they meet the following conditions:

$$r = \frac{T_{FIX} + \alpha}{\alpha} \quad \text{when} \quad N = N_O \tag{17}$$

$$r = \frac{T_{FIX} + \alpha - T_{RES}}{T_{RES} - \alpha} \quad \text{when} \quad N = N_O + 1 \tag{18}$$

$$\text{where } 0 \leq \alpha < T_{RES}. \tag{19}$$

Therefore, the maximum achievable ratio, r_{MAX}, is calculated as follows:

$$r_{MAX} = max\left(\frac{T_{FIX} + \alpha}{\alpha}, \frac{T_{FIX} + \alpha - T_{RES}}{T_{RES} - \alpha}\right), \tag{20}$$

where T_{FIX} is the wall-target distance. Eq. (20) determines the time-resolution or the reference frequency when the HPF order, desired wall-attenuation, wall-target distance, and the bounds of the radar-wall distance have been set. For example, if the demanded ratio is above 4, the wall-target distance is 1.5 m, and the radar-wall distance is within the range of 3 m to 4 m, then the time-resolution is determined to be 5 ns and this is because, this time-resolution always makes a ratio value greater than 4.2 in this case.

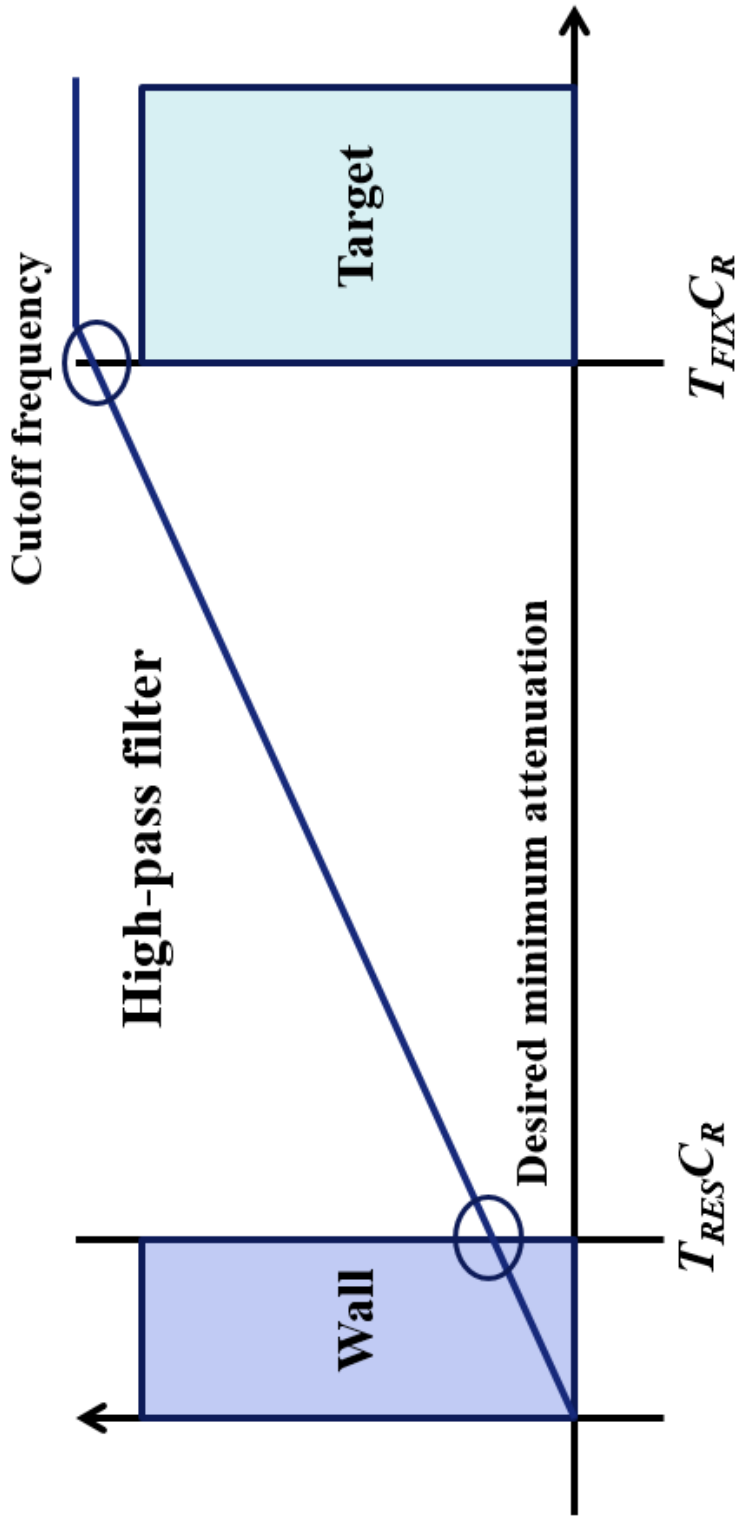

Fig. 17. HPF design methodology.

Although Eq. (20) determines the time-resolution or the reference frequency, it requires some calculation to find the optimum condition and reconfigurable HPF. The modified Eq. (21) and Eq. (22) allow us know the lower boundary of the achievable maximum ratio, $r_{MAX\_LOW\_BOUND}$, and determine a cut-off frequency, f_{CUT_OFF}, of the HPF independently, wherever the wall is located as shown in Fig. 17.

$$r_{MAX\_LOW\_BOUND} = \frac{T_{FIX}}{T_{RES}}, \tag{21}$$

$$f_{CUT\_OFF} = T_{FIX} C_R. \tag{22}$$

Note that in order to design an HPF with conventional FMCW radars, the upper and lower bounds of radar-wall distance and target-wall distance must be pre-defined. However, to design an HPF with the proposed radar system, we only predefine a wall-target distance. For example, when detecting a target located 1.5 m behind a wall, in order to achieve the minimum ratio of 8, the time-resolution is set to 1.25 ns. The HPF cut-off frequency is set to 250 kHz when the chirp rate is 25,000 GHz/s. In the above condition, a second-order HPF with 250 kHz cut-off frequency can

attenuate wall-clutter by at least 30 dB and attenuate target signal by less than 3 dB in all cases where the wall-target distance exceeds 1.5 m.

Note that 400 MHz is a good candidate reference frequency: as it is not a particularly high frequency, many low-cost commercial components available, including phase controller, while the required filter order is only two, to attenuate wall-clutter more than 30 dB where a target located 1.5 m from a wall.

3.3. Measurement results

A radar is implemented to verify the proposed technique. A reference clock is generated by an external signal generator. The reference frequency is chosen as 400 MHz to achieve a 1.25 ns time-resolution. An HMC988LP3E chip [16] is exploited to advance the reference clock entering into a TX PLL. Two LMX2492 chips [17] are used to generate a 9.0-10.0 GHz chirp signal with 40 μs as rising and falling time. The generated TX chirp signal are amplified and emitted by an antenna. The emitted chirp signals propagate in free-space and are reflected by a wall and a target. The reflected chirp signals are amplified and entered into the mixer RF port.

When the LO chirp enters the mixer LO port, the mixer produces a beat-frequency corresponding to the time-gap between the LO chirp and the received signal. The produced beat-frequency signal passes a second-order HPF with a 220 kHz cut-off frequency, and is measured by a spectrum analyzer (MS2830A[18]). Note that any low-pass filter (LPF) was not implemented in the final system for the test. However, the mixer and the spectrum analyzer act like the LPF. The mixer attenuates

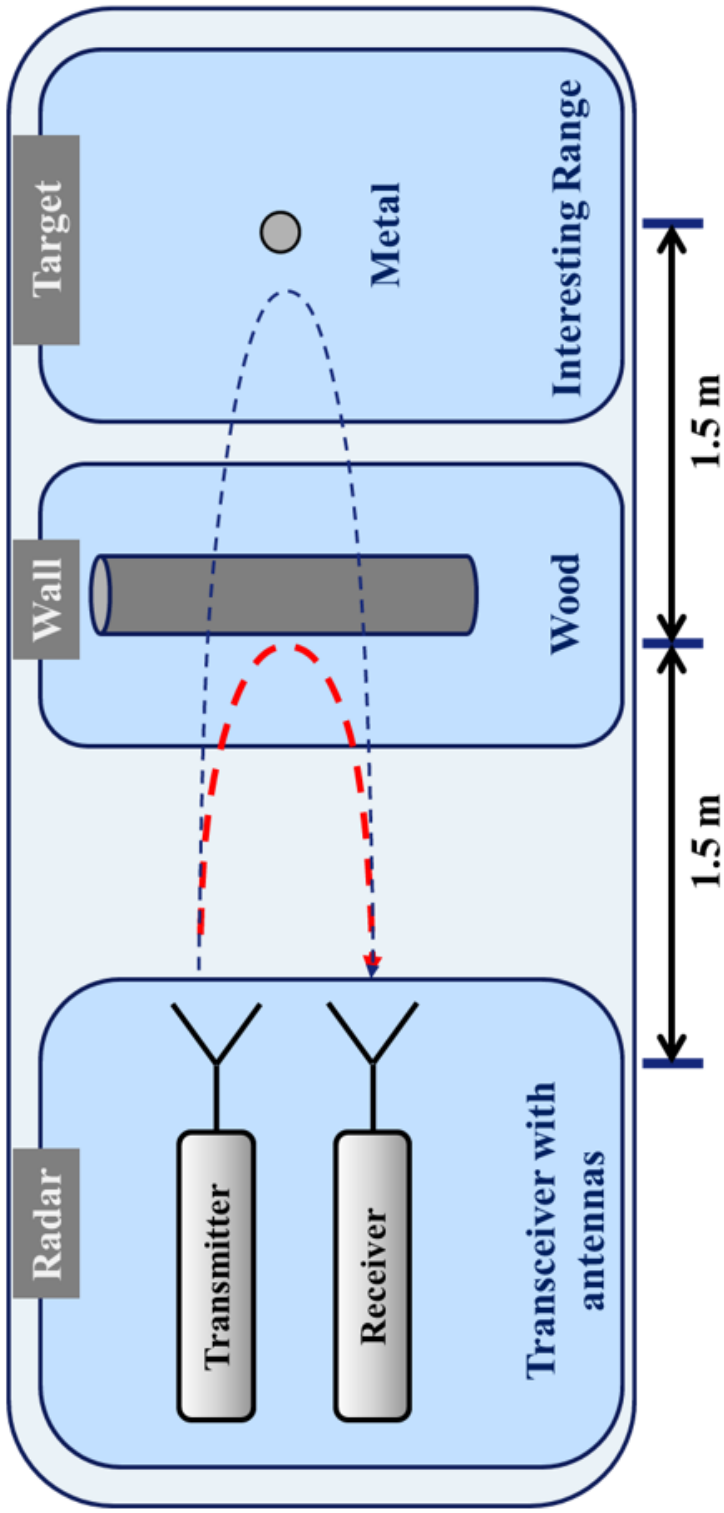

Fig. 18. Measured environment. The wall and the target were middle of the room at 1.5 m and at 3.0 m from radar, respectively.

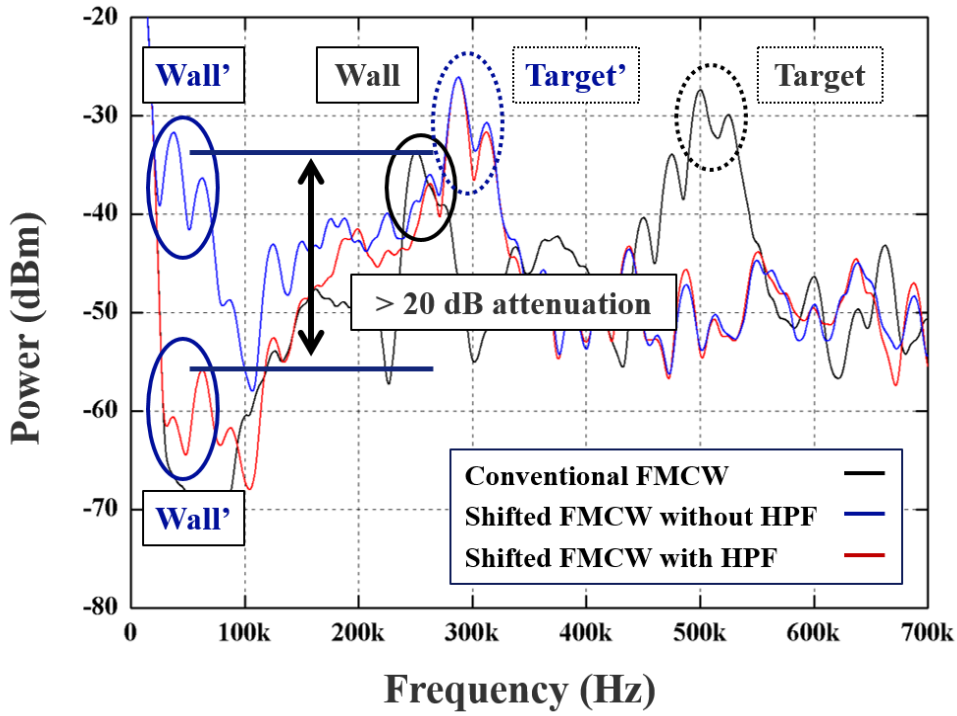

Fig. 19. Measured results. The wall is located at 1.5 m and the target is located at 3 m. Conventional FMCW radar beat-frequency results (black), TX chirp time advanced FMCW radar without HPF beat-frequency results (blue), TX chirp time advanced FMCW radar with HPF beat-frequency results (red) [15].

high-frequency signals such as the sum signal generated during the mixing process. And the spectrum analyzer eliminates out-range frequency signals.

The test was performed in a room. A wall and a target were located at the middle of the room as shown in Fig. 18. Before the measurements, the radar was calibrated. After calibration, the beat-frequencies were measured by the spectrum analyzer. After that, time-shifting was performed and the beat-frequencies were measured by the spectrum without HPF and with HPF. The measured results are shown in Fig. 19.

The wall was located at 1.5 m and the target was located at 3 m. The corresponding beat-frequencies are 250 kHz and 500 kHz with the chirp rate 25,000 GHz/s. After radar calibration process, the measured wall-beat-frequency was 250.8 kHz and the target-beat-frequency was 500.2 kHz. The measured powers were -33.575 dBm and -27.346 dBm, respectively. After the TX chirp time-shift, the beat-frequencies were measured without HPF and with HPF. In the case without HPF, the measured wall-beat-frequencies were 37.4 kHz and 62.6 kHz. The measured powers were -31.679 dBm and -36.31 dBm, respectively. The target-beat-frequency was 287.6 kHz and the power was -26.073 dBm. In the case with HPF, the measured wall-beat-frequencies were

36.8 kHz and 62.8 kHz. The measured powers were −60.623 dBm and −55.842 dBm, respectively. The target−beat−frequency was 287.6 kHz and the power was −26.075 dBm. Note that the wall−beat−frequency signal is attenuated by more than 20 dB while the target−beat−frequency signal is not attenuated by the second−order HPF.

3.4. Conclusion

In this chapter, we propose a novel FMCW radar that strongly attenuates wall-clutter with a low-order HPF by utilizing two PLLs and a phase controller. Additionally, this technique decouples the relationship between the radar-wall distance and the HPF's cut-off frequency. To design an HPF with the proposed system, we only predefine the wall-target distance when a chirp rate and desired wall attenuation are set. The proposed system allows for the use of radars in diverse environments. The measurement results show that a second-order HPF attenuates by more than 20 dB for a wall located at 1.5 m and does not attenuate for a target located at 3 m. The proposed radar is highly appropriate for wall-penetrating detection applications.

Chapter 4

Conclusion

This thesis proposes a novel frequency-modulated continuous-wave (FMCW) radar architectures for through-the-wall radar applications. By combining a delay-line technique and a novel FMCW radar architecture with a low-frequency digital control technique, a low-order high-pass filter (HPF) fully attenuates wall-clutter. Additionally, this technique decouples the relationship between the radar-wall distance and the HPF's cut-off frequency. Therefore, the proposed techniques allow for the use of wall-penetrating radars in diverse environments.

The measurement results show that a second-order HPF attenuates by more than 20 dB for a wall located at 1.5 m and does not attenuate for a target located at 3 m. The proposed radar is highly appropriate for wall-penetrating detection applications.

Also, this architecture can be modified to develop new instruments such as "range-profile-analyzer". Thanks to the reconfigurability of the time-gap between TX chirp and LO chirp, the range scan function can be achieved.

The proposed digital-based time-gap control technique is also applied to other system such as a FMCW radar for altimeter application or a FMCW radar with a very low antenna isolation.

Appendix A

A wideband DC block design for wideband radar applications

This chapter proposes a wideband compact DC block design technique. This DC block has a wide pass-band and wide stop-band and transforms termination impedances. It comprises a pair of coupled lines on a defected ground structure (DGS) with capacitor loading. A periodic DGS pattern increases coupling, and, consequently, a wideband DC block design is allowed with a microstrip process on a high dielectric low height substrate. A DC block with equal termination impedances of 50 Ω and another that transforms 50 into 30 Ω are fabricated. The measured fractional bandwidths are 48% and 47%. The size of the DC block is 16.8 × 15 mm^2 ($0.057\lambda_0 \times 0.051\lambda_0$).

Appendix A.A Introduction

For supporting wideband radar applications, a compact size wideband DC block is required. At the same time, a DC block with an impedance transforming characteristic is required to eliminate an additional matching network for noise matching of an LNA or power matching of a PA [19-20]. In addition, a wide stop-band characteristic is desirable for the receiver design [21]. In previous works, a cymbal type DC block was proposed for a wideband DC block [22]. However, [22] this does not provide an exact DC block design equation and a design method for different termination impedances. Distributed coupled DC block design equations for equal and different termination impedance are provided [23], but the length of the coupled line is fixed at a quarter-wavelength; therefore, this DC block has a long length [20], [23]. Spurious frequency also occurs at the third-harmonic frequency. These problems were overcome in [24]; however, the structure in [24] requires grounded coupled lines or series inductors. The grounded coupled lines cannot be used for DC blocks. The series inductor is an unattractive component because it generally has a poor quality

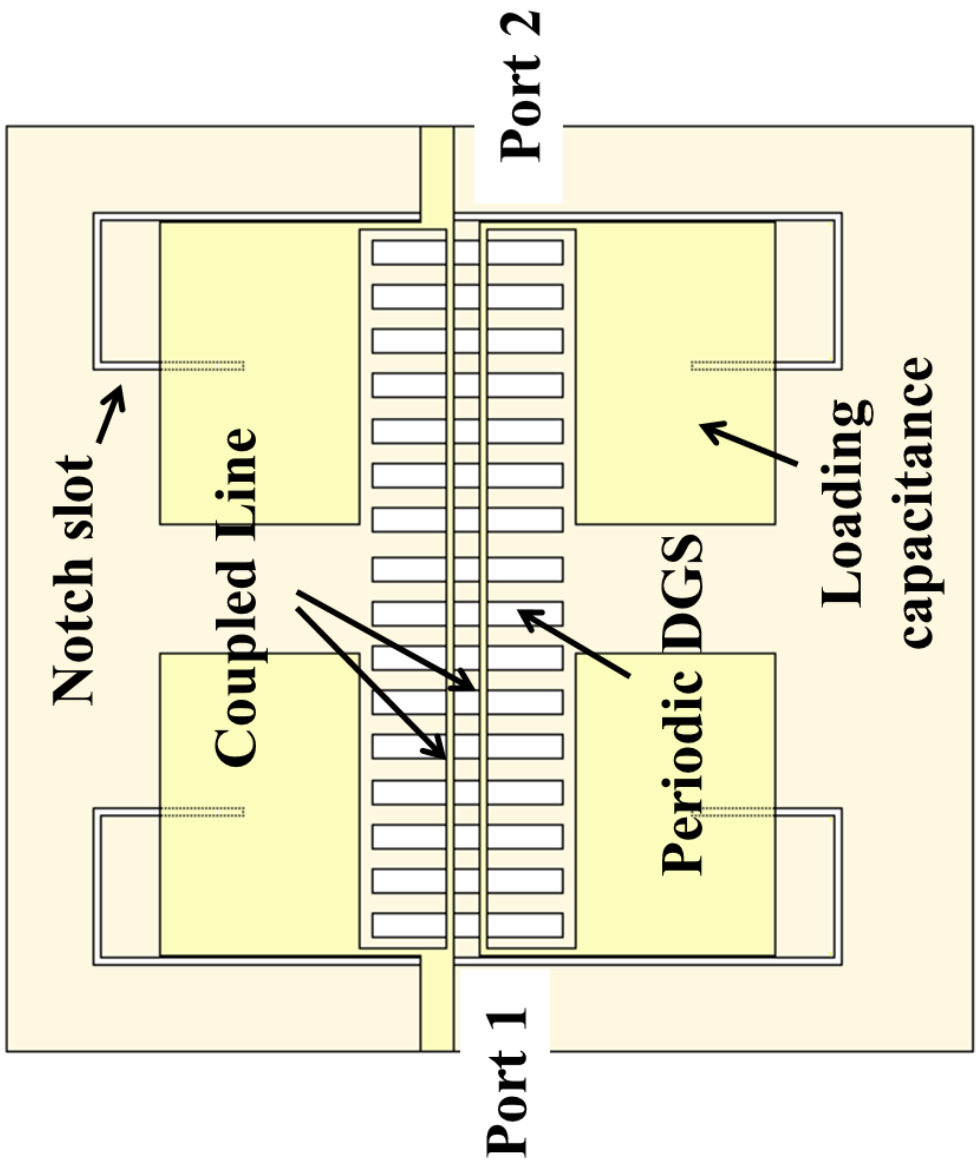
Port 2
Notch slot
Coupled Line
Periodic DGS
Loading
capacitance
Port 1

(a)

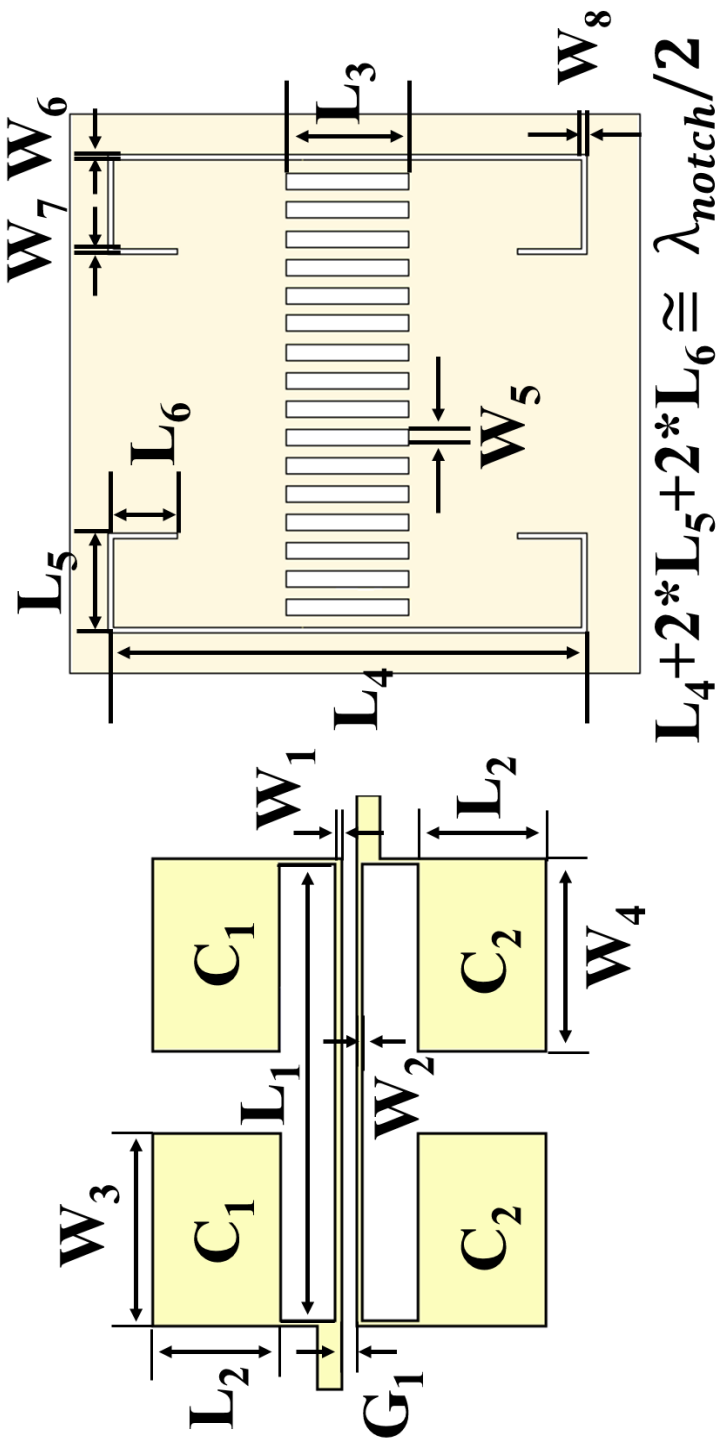

(b)

Fig. 20. The proposed DC block. (a) Overall-view, (b) top-view, and bottom-view [25].

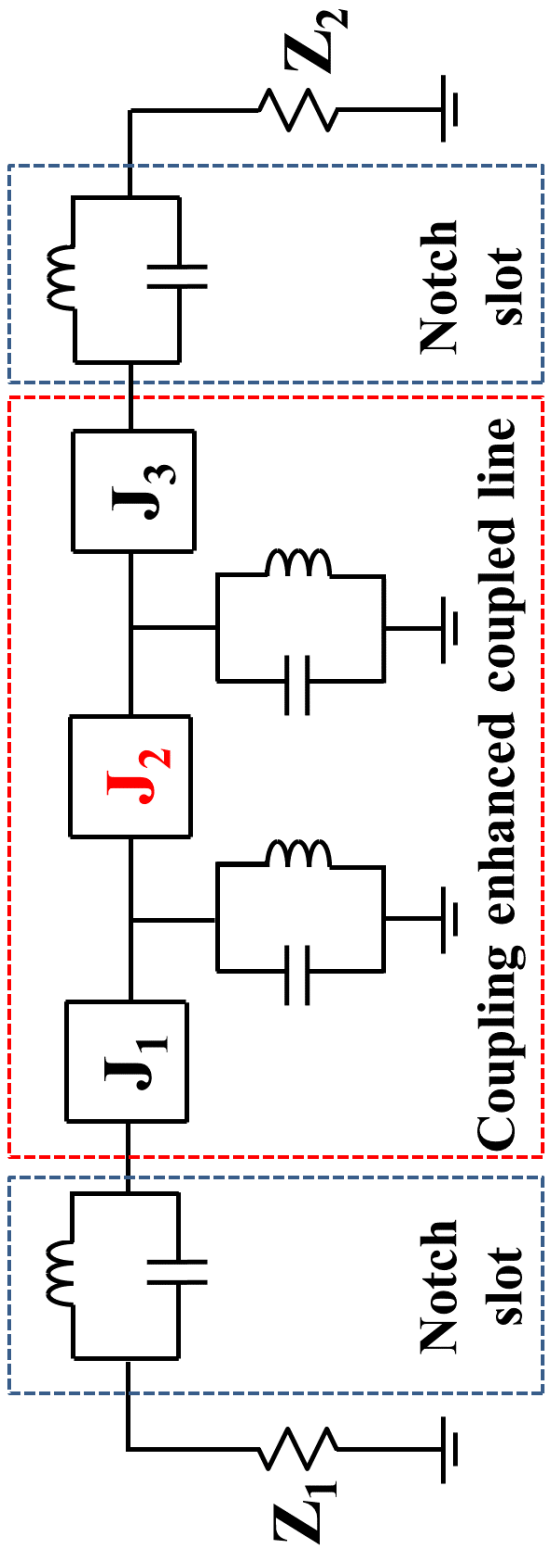

Fig. 21. The equivalent circuit of the proposed DC block [25].

factor and its maximum value is limited in fabrication [23]. Moreover, the bandwidth is limited because the maximum mutual coupling coefficient is restricted by a given substrate and microstrip process [23]. It becomes more problematic when using a high dielectric, low height substrate for compact DC block design.

In the present study, a defected ground structure (DGS) is exploited to overcome these problems. A periodic DGS not only makes a slow wave but also enhances coupling between a pair of coupled lines. A slow wave allows a compact DC block design, and an enhanced coupling coupled line allows a wideband DC block design on a high dielectric low height substrate. Capacitance loaded transmission lines and DGS slots are also exploited to attain a more compact DC block and to increase stop-band.

A periodic DGS, transmission lines and the loading capacitors are modeled by two resonators with enhanced coupling (J_2) compared with conventional structure. Therefore, if we assume the notch slots have little effect on pass-band operation, then the general second order filter design equation can be directly applied, and this filter design equation allows us to know all the design parameters when the termination impedances, bandwidth, and the filter type are determined. The proposed DC block is shown in Fig. 20 and the equivalent circuit is shown in Fig. 21.

Appendix A.B Analysis and design

For a wideband DC block design, a high coupling structure is needed. In [26], a large square aperture structure is proposed to enhance the coupling. However, this increases the circuit size due to its high wave propagation velocity. In this study, we focus on a periodic square DGS pattern to enhance the coupling while decreasing wave propagation velocity for a compact DC block.

DGS patterns are normally used to achieve a filtering effect or slow wave effect. However, in this study, we focus on a periodic DGS pattern to increase the coupling between two coupled lines. This DGS pattern makes the larger the difference between the even- and odd-mode impedance. Consequently, it increases coupling between two coupled lines. A square DGS pattern is considered a suitable pattern; due to its layout shape that allows several slots to be easily inserted in restricted area, and the width and length of the slots to be easily adjusted. Therefore, slow wave factor and coupling magnitude are controlled with ease.

For more compact size DC block design, a capacitance loading technique is adopted. It helps to decrease the transmission line length and expand the stop-band [27]. However, stop-band

expansion is limited due to the loading capacitor value being restricted by its size. Therefore, the notch slots are also used for stop-band expansion. These slots act like a notch filter. Folded type slots are used to design a compact size DC block.

For a proposed DC block implementation, first, we investigate the characteristic impedance Z_0 and the electric length θ of the transmission line on a periodic DGS slots. It can be carried out by an EM simulation.

Second, we obtain loading capacitor values. The capacitance of the patch, C_1, is determined by

$$C_1 = \frac{1}{2\pi f_0 Z_0 \tan(\frac{\theta}{2})} \tag{23}$$

where f_0 is the center frequency. C_2 is also determined using the same equation.

Third, we decide the initial parameter. The following design equations can be used for determining the initial parameter values.

$$Q_1 = \frac{g_0 g_1}{FBW}, \tag{24}$$

$$Q_2 = \frac{g_2 g_3}{FBW}, \tag{25}$$

$$M_{12} = \frac{FBW}{\sqrt{g_1 g_2}} \tag{26}$$

where g_0, g_1, g_2, and g_3 are the low-pass prototype parameters, given for a normalized low-pass cutoff frequency $\Omega_c = 1$, Q_1, and Q_2 are the external quality factors of the resonators, FBW is the fractional bandwidth, and M_{12} is the coupling coefficients between the resonators. DC blocks have the same operation if these initial parameters are same. This implies that impedance transform can be achieved by meeting these initial parameters.

Due to the external qualify factor of each resonator being proportional to the termination impedance, when the termination impedance is lower, the transmission line width of the resonator with lower termination impedance must be extended for increasing susceptance slope. In the opposite case, the line width must be shrunk.

Finally, we insert DGS notch slots, which are shown in Fig. 16. These slots increase the stop-band. These notch slots are modeled by a series connected parallel resonators. A bent-slot is used to reduce the area of the circuit. The total length of the notch slots, L_4

$+2L_5 + 2L_6$, is equal to $\lambda_{notch}/2$, where λ_{notch} is the wavelength at the notch frequency. The simulated results (50-50 Ω terminated DC block with/without slots) show that the stop-band (S_{21} 20dB attenuation reference) is extended to around 850 MHz, which corresponds to 85% of the center frequency.

The proposed DC block has a large ratio of notch-band frequency to pass-band frequency due to its use of the periodic DGS pattern and capacitance loading. Therefore, these notch slots rarely affect pass-band operation. However, in case these notch slots significantly affect pass-band performance, a physical parameter modification and optimization step is required to meet the bandwidth.

Appendix A.C Implementation and measurements

The feasibility of the proposed wideband DC block is verified through measurements of a design consisting of one DC block with 50 Ω to 50 Ω termination impedances and another one transforming 50 into 30 Ω at the center frequency of 1 GHz. They are fabricated on a high dielectric, low height, highly lossy substrate (FR−4 substrate, with ε_r = 4.6, H = 0.2 mm and tan δ = 0.25). The design parameters are shown in TABLE I. The fabricated circuits are shown in Fig. 22, and the simulated results are compared with the measured ones in Fig. 23. The simulation and measurement results are well matched in both cases. The measured S_{21}s are −0.79 dB and −0.91 dB around the center frequency, and the 3−dB bandwidths are 0.80−1.29 GHz and 0.806−1.286 GHz (48% and 47%), respectively. The proposed DC block accomplishes wideband performance and the corresponding coupling coefficient on a high dielectric, low height substrate and the gap (G_1) of two coupled lines is wide (0.8 mm). It implies that the proposed structure has successfully solved the coupling strength problem. The insertion loss looks slightly high, since an FR−4 substrate is a highly lossy material. The size of the proposed DC blocks are 16.8

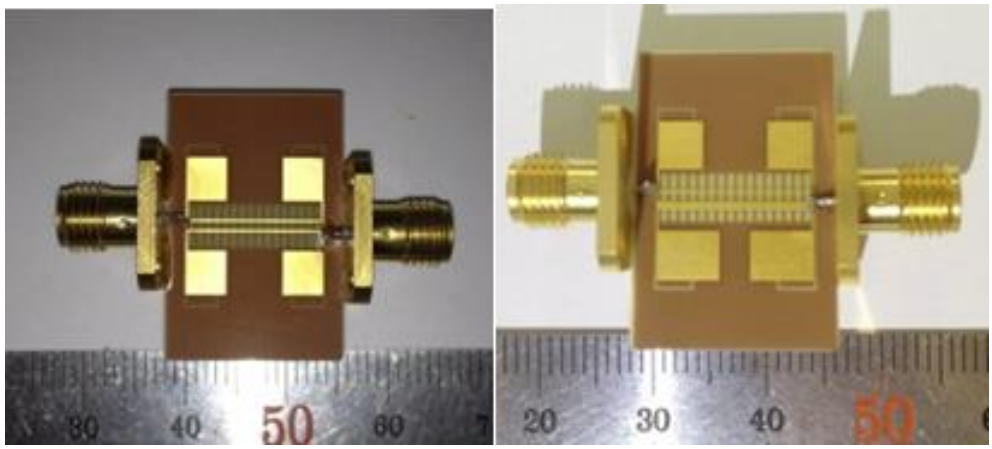

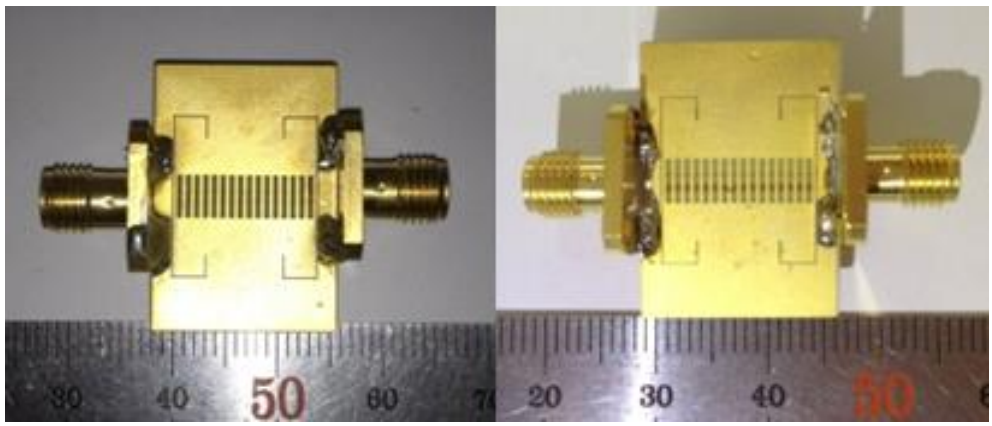

Fig. 22. The fabricated DC blocks. (a), (c) : 50 and 50 Ω terminated DC block top and bottom view. (b), (d) : 50 and 30 Ω terminated DC block top and bottom view [25].

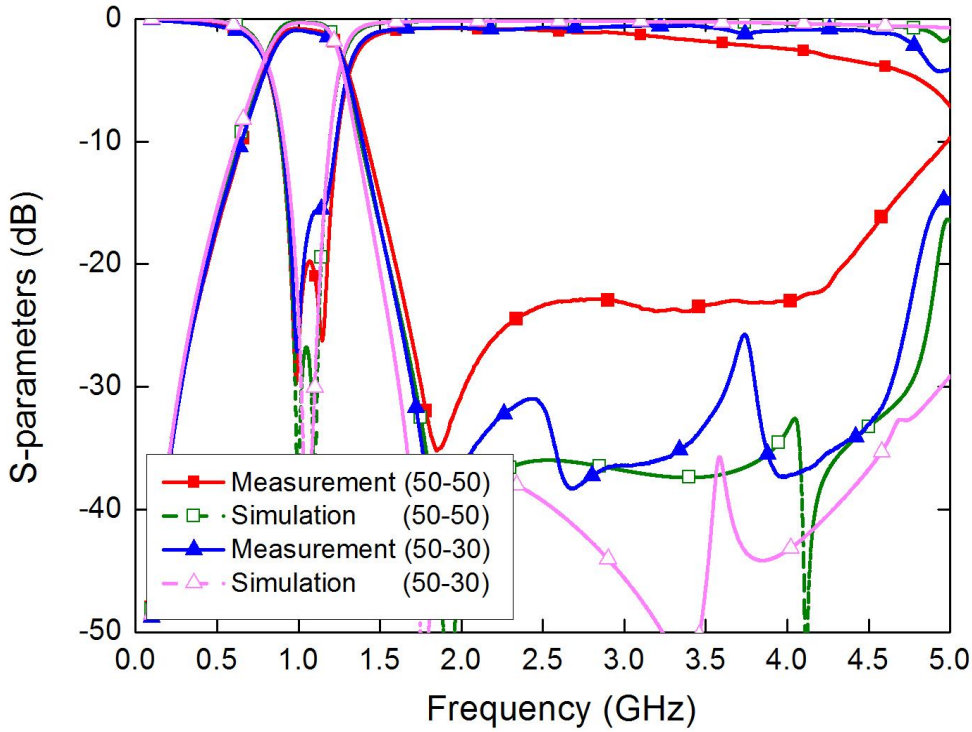

Fig. 23. The simulation and measurement results: 50 and 50 Ω terminated DC block and 50 and 30 Ω terminated DC block [25].

TABLE I. Design parameters

Unit : mm	50 - 50 Ω terminated	50 - 30 Ω terminated
W_1	0.15	0.15
W_2	0.15	0.6
L_1	12.8	12.8
G_1	0.8	0.8
W_3	3.75	3.75
W_4	3.75	5.15
L_2	4	4
W_5	0.52	0.52
L_3	4	4
$W_6 = W_7 = W_8$	0.15	0.15
L_4	15	15
L_5	3.15	3.15
L_6	2.15	2.15

TABLE II. Comparitve summary about the bandwidth, size, impedance transformation, filter type and gap (G_1) of DC blocks

	FBW (%)	Size ($\lambda_0 \times \lambda_0$)*	Impedance transformation	Filter type	gap (mm)
This work	47	$0.057\lambda_0 \times 0.051\lambda_0$	O	Butterworth	0.8
Ref. [22]	10	$0.387\lambda_0 \times 0.134\lambda_0$	X	Not Specified	0.37
Ref. [23]	50**	$0.008\lambda_0 \times 0.17\lambda_0$	O	Butterworth	0.25
Ref. [24]	9.2	$0.237\lambda_0 \times 0.169\lambda_0$	Not Specified	Chebyshev	Not Specified

* λ_0 is the wavelength in the free space at the center frequency.
** FBW is estimated by figure.

$\times$ 15 mm^2 ($0.057\lambda_0 \times 0.051\lambda_0$), where λ_0 is the wavelength in the free space at the center frequency. TABLE II gives a summary about the bandwidth, size, impedance transformation, filter type and gap of DC blocks.

Appendix A.D Conclusion

In this chapter, we have introduced a new DC block structure. It has wide pass-band, wide stop-band, and an impedance transforming property with compact size. This structure successfully overcomes the coupling strength problem by exploiting a periodic DGS. One DC block with equal termination impedance and another with unequal termination impedance were fabricated and measured. They have 48% and 47% fractional bandwidth, respectively. The measurement results tally with the simulation results. The proposed DC block is appropriate for compact microwave components and monolithic microwave integrated circuits (MMICs).

Appendix B

Detailed FMCW radar components in chap. 3

Appendix B.A High-pass filter

In the measurement, a second-order HPF was used to attenuate wall-clutter. The implemented filter was Butterworth type HPF with 220 kHz cut-off frequency. Theoretically to realize the HPF, a 28.17 μH shunt inductor and a 11.27 nF series capacitor are required. And the HPF measurement responses should be reciprocal, because the HPF is passive network.

However, the whole block's responses can be changed and not be reciprocal because the mixer's responses can be changed related with its load impedance. Therefore, the mixer's load impedance should be considered, when the user adopts the response variation mixer related with its load impedance.

In the proposed radar implementation, a 30 μH shunt inductor and a 12 nF series capacitor were used accounting with the mixer's response. The Fig. 24 shows frequency responses. The filter frequency responses (black and red) show a reciprocal

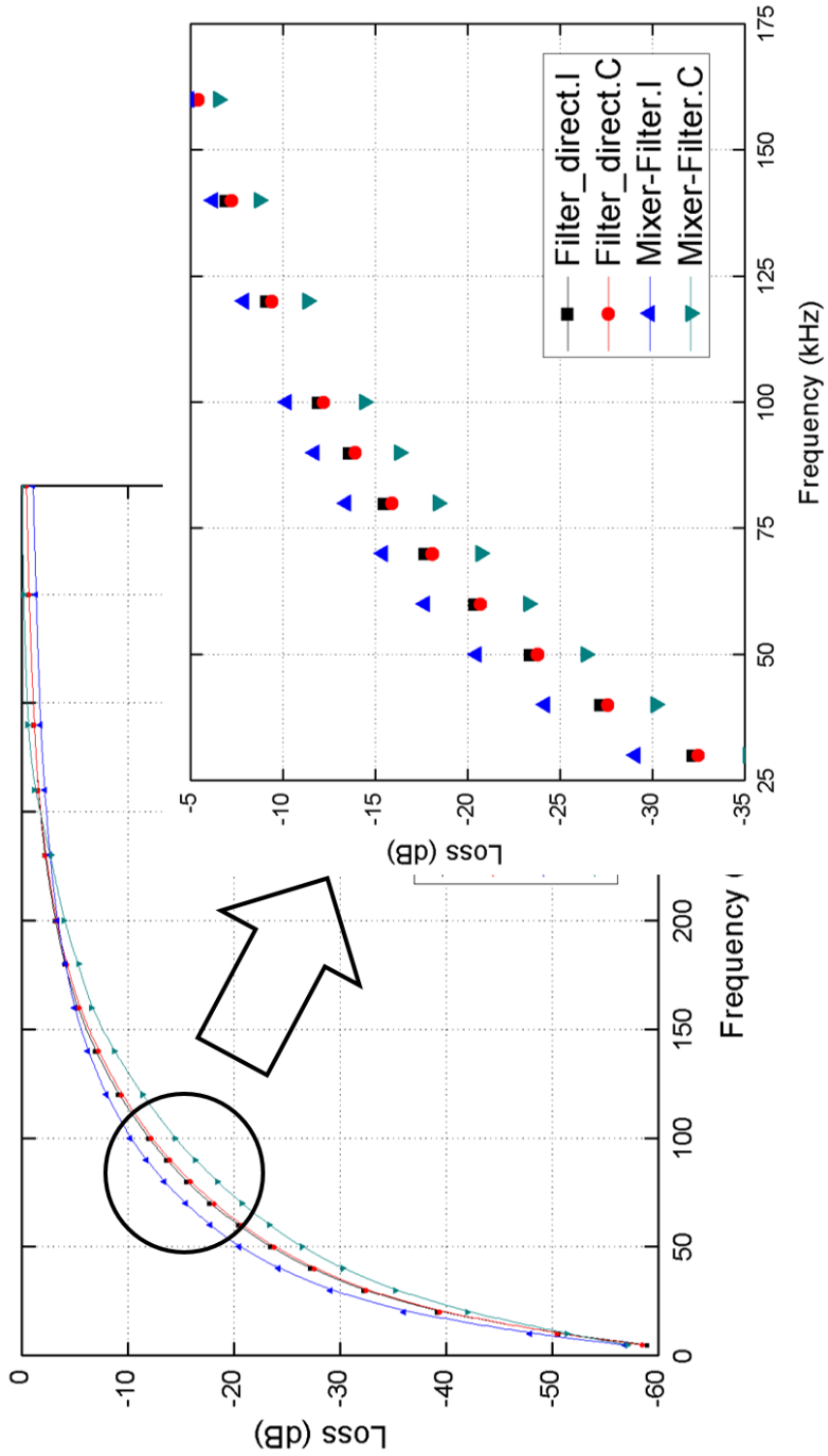

Fig. 24. Measurement results. Filter only response (black and red) and filter with mixer response (blue and green) [28].

characteristic. However, the filter with mixer frequency responses (blue and green) show not a reciprocal characteristic. Therefore, when design the HPF, consideration of the mixer's responses variation depending on its load condition (i.e. HPF's input impedance) is important.

The measurement results show that a filter with mixer combined block has 220 kHz cut-off frequency when the mixer's load is connected with shunt inductor firstly. Therefore, the consideration of a mixer's response variation is important when the user uses a response variation mixer depending on its load condition and the mixer is connected with the filter directly.

Appendix B.B Chirp source

In short-range FMCW radar applications, not only chirp source frequency linearity but also its amplitude and phase noise are important.

The chip, LMX2492 [17], is used as a chirp source. This chip provides high speed chirp function with a high performance. The fig. 25 shows that a phase noise of the PLL provided from the manufacturer [17]. This figure shows that the phase noise is approximately −97.9 dBc/Hz at 1 kHz, −106.3 dBc/Hz at 10 kHz, −111.5 dBc/Hz at 100 kHz, and −115.5 dBc/Hz at 1 MHz when the center frequency was 4.8 GHz.

The phase noise was measured at 9.8 GHz with an external sine input source. The measured value was approximately 10 dB worse than the provided data sheet which was measured at 4.8 GHz. The measured phase noise was aprroximately −84 dBc/Hz at 1 kHz, −92 dBc/Hz at 10 kHz, −92 dBc/Hz at 100 kHz, and −102 dBc/Hz at 1MHz.

The measured amplitude is shown in fig. 26. The output varies within −2.6 dBm to 0.5 dBm in range of 9.0-10.0 GHz. Other components such as an amplitude limiter and frequency divider can decrease the amplitude variation.

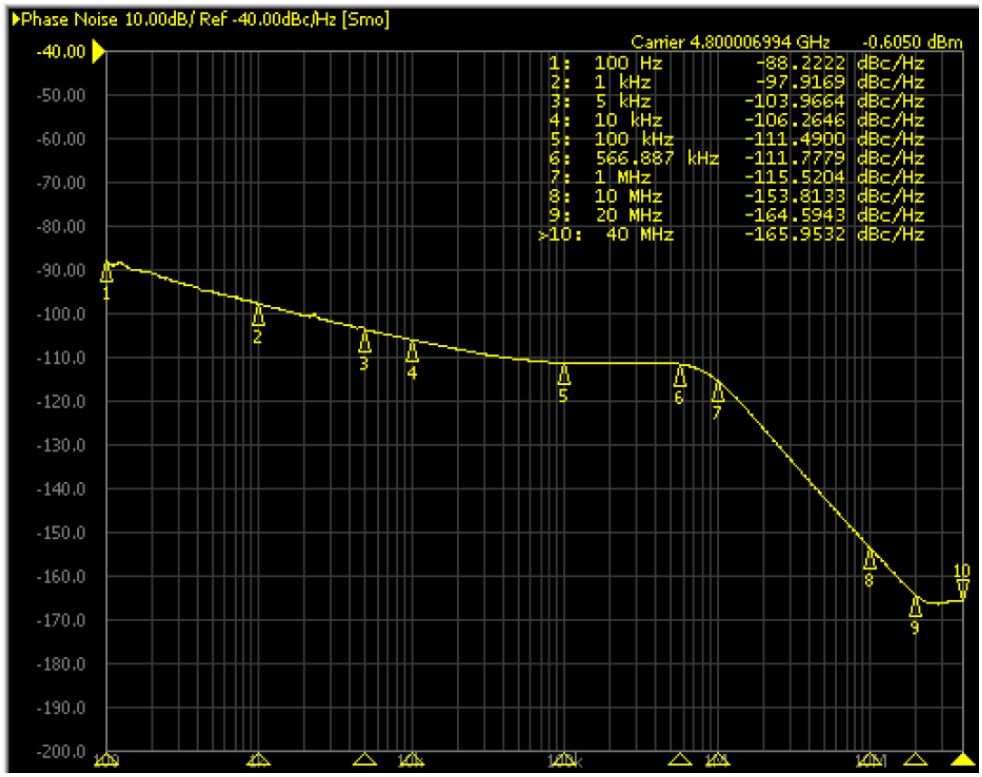

Fig. 25. Phase noise of the PLL [17].

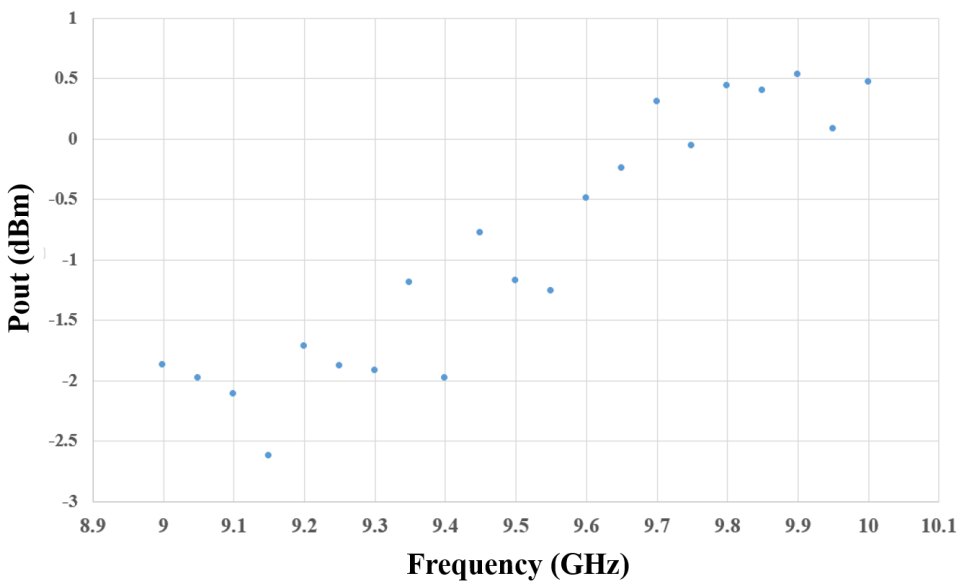

Fig. 26. Output power of the PLL.

The required frequency linearity, phase noise and amplitude uniformity are determined by operation scenario.

Bibliography

[1] Y. Lim and S. Nam, "Target-to-clutter ratio enhancement of images in through-the-wall radar using a radiation pattern-based delayed-sum algorithm," *Journal of Electromagnetic Engineering and Science*, vol. 14, no. 4, pp. 405-410, Dec. 2014.

[2] Y. Yang and A. E. Fathy, "See-through-wall imaging using ultra wideband short-pulse radar system," in *Proc. IEEE Antennas Propag. Soc. Int. Symp.*, pp. 334-337, 2005.

[3] G. L. Charvat, L. C. Kempel, E. J. Rothwell, C. M. Coleman, and E. L. Mokole, "A through-dielectric radar imaging system," *IEEE Trans. Antennas Propag.*, vol. 58, no. 8, pp. 2594-2603, Aug. 2010.

[4] N. Maaref, P. Millot, C. Pichot, and O. Picon, "FMCW ultra-wideband radar for through-the-wall detection of human beings," in *Proc. Int. Radar Conference - Surveillance for a Safer World*, pp. 1-5, Oct. 2009.

[5] B. R. Mahafza, *Radar Systems Analysis and Design Using MATLAB*, 2000 : Chapman Hall/CRC

[6] B. Kim et al., "A Clutter Rejection Technique Using a Delay-line for Wall-penetrating FMCW Radar," *IEICE Trans. Electron*, vol. E99-C, no. 5, pp. 597-600, 2016.

[7] L. Reindl, et al., "Design, fabrication, and application of precise SAW delay lines used in an FMCW radar system," *IEEE Trans. Microw. Theory Tech.*, vol. 49, no. 4, pp. 787-794, April 2001.

[8] M. M. Jatlaoui, et al., "Original identification technique of passive EM sensors using loaded transmission delay lines," in *Proc. EuMC*, pp. 1106-1109, Sep. 2010.

[9] J. H. Choi, J. H. Jang and J.E. Roh, "Optical-delay-based wide-range FMCW radar altimeter," *Elect. Lett.*, vol. 50, no. 25, pp. 1975-1977, Dec. 2014.

[10] J. S. Hong and M. J. Lancaster, *Microstrip Filters for RF/Microwave Applications*, 2001 : Wiley

[11] ADS (Advanced Design System: Keysight Technologies) [Online]. Available at: http://www.keysight.com/en/pc-1297113/advanced-design-system-ads?cc=KR&lc=kor/

[12] B. Kim, et al., "A dual-band FMCW radar for through-wall detection," in *Proc. 2015 Asia-Pac. Conf. Synth. Aperture Radar (APSAR)*, Sep. 2015, pp. 54-57.

[13] D. M. Pozar, Microwave Engineering 3rd ed., 2005 : Wiley

[14] H.D. Griffiths, "The effect of phase and amplitude errors in FM radar," in *IEE High Time-Bandwidth Product Waveforms in Radar Sonar Colloq.*, London, U.K., 1991, pp. 9/1-9/5.

[15] B. Kim, et al., "A Wall-Clutter Rejection Technique using Two PLLs and a phase controller for Wall-Penetrating FMCW Radar," *IEEE Geoscience and Remote Sensing Letters*, (on publication process).

[16] Analog Device [Online]. Available: http://www.analog.com/en/index.html

[17] Texas Instruments [Online]. Available: http://www.ti.com/product/LMX2492

[18] Anritsu [Online]. Available: https://www.anritsu.com

[19] H.-R. Ahn and B. Kim, "Toward integrated circuit size reduction," *IEEE Microw. Mag.*, vol. 9, no. 1, pp. 65-75, Feb. 2008.

[20] M. Abbasi, H. Zirath, and I. Angelov, "Q-, V-, and W-band power amplifiers utilizing coupled lines for impedance matching," in *Proc. IEEE MTT-S International Microwave Symposium Digest*, Jun. 15-20, 2008, pp. 863-866.

[21] A. A. Abidi, "The path to the software-defined radio receiver," *IEEE J. Solid-State Circuits*, vol. 42, no. 5, pp. 954-966, May 2007.

[22] B. Strassner and K. Chang, "New wide-band DC-block cymbal bandpass filter," *IEEE Trans. Microw. Theory Tech.*, vol. 50, no. 5, pp. 1431–1432, May 2002.

[23] H.-R. Ahn and T. Itoh, "Impedance-transforming symmetric and asymmetric DC blocks," *IEEE Trans. Microw. Theory Tech.*, vol. 58, no. 9, pp. 2463–2474, Sep. 2010.

[24] S. Lee and Y. Lee, "Generalized miniaturization method for coupled-line bandpass filters by reactive loading," *IEEE Trans. Microw. Theory Tech.*, vol. 58, no. 9, pp. 2383-2391, Sep. 2010.

[25] B. Kim, et al., "Design of wideband coupled line DC block with compact size," *IEICE Trans. Electron*, vol. E97.C(9), pp. 915-917, 2014.

[26] L. Zui, H. Bu, and K. Wu, "Aperture compensation technique for innovative design of ultra-broadband microstrip bandpass filter," *IEEE MTT-S Int. Microwave Symp. Dig.*, Boston, MA, pp. 315-318, June 2000.

[27] J.-S. Hong and M. J. Lancaster, "Theory and experiment of novel microstrip slow-wave open-loop resonator filters," *IEEE. Trans. Microw. Theory Tech.*, vol. 45, no. 12, pp. 2358-2365, Dec. 1997.

[28] 김병준, 구종섭, 김덕수, 남상욱, "A HPF Design Technique for Wall-clutter Attenuation," 2016년 한국전자파학회 하계종합학술대회, 2016년 6월.

초록

이 논문은 벽투과용 FMCW레이다를 위한 벽클러터 제거기법과 새로운 레이다구조를 제시했다. 벽투과파에 의해 수신기와 ADC의 높은 동적영역이 필요하므로 벽투과 레이다 응용에서, 벽클러터 제거는 매우 중요하다. 광대역 FMCW레이다는 좋은 고해상도 벽투과 탐지레이다 후보 중 하나인데, IF대역이나 기저대역에서 벽클러터를 충분히 제거할 수 있는 레인지게이팅 필터를 사용함으로써 높은 동적 범위를 확보할 수 있기 때문이다. 그러나, 호모다인 FMCW레이다에서는 벽 뒤 멀지 않은 곳에 표적이 있는 경우 벽클러터를 충분히 제거하기 위해서는 매우 높은 차수의 고주파대역통과필터가 요구된다.

이 논문에서 우리는 먼저 지연선로 기법에 관하여 연구한다. 지연선로는 수신신호와 첩신호 사이의 시간차이를 줄인다. 그러므로 타겟과 벽에 의한 비트 신호들의 주파수가 낮아지며 통과대역 대비 저지대역 주파수 비가 증가한다. 그 결과, 낮은 차수의 고주파대역통과필터가 필터 요구사항을 만족시킬 수 있다. 디자인 기법과 근거리 표적이 있는 경우에 대한 예시가 이 논문에서 제공된다. 그리고 그 유효성은 시스템 전산모의에 의해 검증되었다.

비록 지연선로 기법이 낮은 차수의 고주파대역통과필터를 통해서도 벽클러터를 충분히 제거할 수 있게하나, RF나 LO신호 경로에 지연선로를 사용하는 것은 몇가지 문제점을 발생시킨다: 1) 통상적으로 긴 지연선로는 X대역이나 Ka대역과 같은 고주파대역에서 큰 신호

손실을 발생시킨다; 2) 이런 손실이 주파수 의존적이므로 신호손실은 의도치않은 진폭변조도 발생시킨다. 그러므로, 이런 진폭변조는 레이다 대역폭이 증가함에 따라 크게되고, 이는 특히나 고해상도 레이다에서 더욱 문제가 된다. 이런 진폭변조는 표적 비트 신호 근처에 큰 사이드로브를 발생시킬 수 있다; 3) 지연선로는 매우 큰 면적의 단일층 기판이나 긴 지연시간을 발생시키기 위한 특수 공정(예를들어 SAW공정)을 가지고 있는 다층기판을 필요로한다; 4) 짧은 지연부터 긴 지연까지 정밀한 시간조절 분해능을 가지는 조절가능한 지연을 얻기 어렵다. 이것은 매우 많은 지연선로들, 제어회로들, 손실보상회로들을 필요로하고 결국 부피가 큰 시스템이 된다.

그러므로 우리는 두 개의 PLL과 한 개의 위상 조절기를 사용하는 새로운 FMCW레이다 구조를 제안한다. 하나의 PLL은 송신첩신호를 생성하고 다른 하나는 혼합기에서의 혼합을 위한 LO첩신호를 생성한다. 이 PLL들은 기준클럭을 공유하나 송신기 PLL의 입력 경로에는 디지털 위상제어기가 있다. 디지털 위상제어 기능이 동작할 때 제어기는 하나의 에지 신호를 더 생성하고 이후 뒤따르는 에지 신호들을 반전시킴으로써 기준신호를 반주기만큼 빠르게 한다. 각 기준클럭은 2분주되어 각각의 PLL 되먹임클럭과 비교된다. 위상조절기가 반주기만큼 빠르게할 경우 송신기 PLL은 추적을 시작한다. 몇 주기 후, PLL이 빨라진 클럭에 고정되는데 이것은 결국 송신첩 신호를 그 만큼 빠르게 한다. 이런 과정(기준클럭을 빨리하면 PLL이 추적을 시작하고 PLL이 결국 빨라진 클럭에 고정되는 과정)을 반복함으로써 이론상으로는 무한대의

시간차이도 생성할 수 있다. 현실적으로는 송신첩과 LO첩의 유한한 주기로 인해 최대 시간차이가 제한된다. 이런 방법은 위에 언급된 모든 문제를 해결할 수 있다: 이것은 어떠한 RF나 LO신호 손실을 발생시키지 않으며 그러므로 광대역 FMCW레이다의 경우에도 어떠한 진폭변조도 추가로 발생시키지 않는다; 부피를 크게 증가시키지 않는다; 그리고 무한대의 시간지연과 정밀한 시간분해능을 얻을 수 있다. 이 기법은 낮은 차수의 고주파대역통과필터가 벽클러터를 큰 폭으로 감쇄시킬 수 있게 할 뿐만 아니라 벽의 거리와 고주파대역통과필터의 컷오프 주파수 사이의 관계를 분리시킨다. 제안한 레이다를 제작하고 측정하였다. 방 중앙에 레이다로부터 1.5 m 위치에 벽을, 3 m 위치에 표적을 놓았다. 측정결과 이차 고주파대역통과필터가 벽에 의한 비트 신호는 20 dB 이상 감쇄시키는 동시에 표적에 의한 비트 신호는 감쇄시키지 않았다. 제안한 레이다는 벽투과 탐지 응용들에 매우 적합하다.

키워드 : FMCW 레이다, 낮은 차수 고주파대역통과필터, 두 개의 PLL, 벽클러터 제거, 위상 조절기

학번 : 2009-23088